# Paleozoic origins of cheilostome bryozoans and their parental care inferred by a new genome-skimmed phylogeny

**Short title:** Paleozoic origin of cheilostomes

Russell J.S. Orr[1*], Emanuela Di Martino[1], Mali Ramsfjell[1], Dennis P. Gordon[2], Björn Berning [3], Ismael Chowdhury[4], Sean Craig[4], Robyn L. Cumming[5], Blanca Figuerola[6], Wayne Florence[7], Jean-Georges Harmelin[8], Masato Hirose[9], Danwei Huang [10], Sudhanshi S. Jain[10], Helen L. Jenkins[11,12], Olga N. Kotenko[13], Piotr Kuklinski[14], Hanna E. Lee[4], Teresa Madurell[6], Linda McCann[15], Hanna L. Mello[16], Matthias Obst[17], Andrew N. Ostrovsky[13, 18], Gustav Paulay[19], Joanne S. Porter[20], Natalia N. Shunatova[13], Abigail M. Smith [16] , Javier Souto-Derungs[18], Leandro M. Vieira[12,21], Kjetil L. Voje[1], Andrea Waeschenbach[12], Kamil Zágoršek[22], Rachel C.M. Warnock[23], Lee Hsiang Liow[1,24**]

Corresponding author emails: *russell_orr@hotmail.com and **l.h.liow@nhm.uio.no

[1]Natural History Museum, University of Oslo, Oslo, Norway.

[2]National Institute of Water and Atmospheric Research, Wellington, New Zealand.

[3]Geoscience Collections, Oberösterreichische Landes-Kultur GmbH, Linz, Austria.

[4]Department of Biological Sciences, Humboldt State University, Arcata, CA, USA.

[5]Museum of Tropical Queensland, Townsville, Australia.

[6]Institute of Marine Sciences (ICM-CSIC), Barcelona, Spain.

[7]Department of Research and Exhibitions, Iziko Museums of South Africa, Cape Town, South Africa.

[8]Station marine d'Endoume, OSU Pytheas, MIO, GIS Posidonie, Université Aix-Marseille, Marseille, France.

[9]School of Marine Biosciences, Kitasato University, Kanagawa, Japan.

[10]Department of Biological Sciences, National University of Singapore, Singapore.

[11]Marine Biological Association of the UK, Plymouth, UK.

[12]Natural History Museum, London, UK.

[13]Department of Invertebrate Zoology, Faculty of Biology, Saint Petersburg State University, Russia.

[14]Institute of Oceanology, Polish Academy of Sciences, Sopot, Poland.

[15]Smithsonian Environmental Research Centre, CA, USA.

[16]Marine Science, University of Otago, Dunedin, New Zealand.

[17]Department of Marine Sciences, University of Gothenburg, Sweden.

[18]Department of Palaeontology, Faculty of Earth Sciences, Geography and Astronomy, University of Vienna, Austria.

[19]Florida Museum of Natural History, Florida, USA.

[20]International Centre for Island Technology, Heriot Watt University, Stromness, United Kingdom.

[21]Department of Zoology, Universidade Federal de Pernambuco, Recife, Brazil.

[22]Department of Geography, Technical University of Liberec, Liberec, Czech Republic.

[23]GeoZentrum Nordbayern, Friedrich-Alexander-Universität Erlangen-Nürnberg, Germany.

[24]Centre for Ecological and Evolutionary Synthesis, Department of Biosciences, University of Oslo, Oslo, Norway.

**Abstract**

Phylogenetic relationships and the timing of evolutionary events are essential for understanding evolution on longer timescales. Cheilostome bryozoans are a group of ubiquitous, species-rich, marine colonial organisms with an excellent fossil record, but lack phylogenetic relationships inferred from molecular data. We present genome-skimmed data for 395 cheilostomes and combine these with 315 published sequences to infer relationships and the timing of key events among c. 500 cheilostome species. We find that named cheilostome genera and species are phylogenetically coherent, rendering fossil or contemporary specimens readily delimited using only skeletal morphology. Our phylogeny shows that parental care in the form of brooding evolved several times independently, but was never lost in cheilostomes. Our fossil-calibration, robust to varied assumptions, indicates that the cheilostome lineage and parental care therein could have Paleozoic origins, much older than the first known fossil record of cheilostomes in the Late Jurassic.

**Teaser:** The origins of cheilostome bryozoans and parental care in this group are substantially older than previously thought

**Keywords:** genome-skimming, metazoans, Lophotrochozoa, Bryozoa, fossil-calibration, embryonic incubation, speciation

## Introduction

Quantifying macroevolutionary processes, for example diversification rates, and testing macroevolutionary hypotheses, such as whether speciation rate shifts are driven by environmental changes and/or trait evolution, require robust reconstructions of the genealogical relationships of the members of the clade in question. It is increasingly clear that it is preferable to reconstruct evolutionary histories based on both extant and extinct organisms (*1*, *2*) and to combine morphological and molecular data (*3*, *4*). Yet, empirical datasets that combine molecular, morphological and substantial amounts of fossil data are still rare. This is in part because molecular sequencing efforts have been disproportionately focused on organisms with relatively poor fossil records (e.g. birds, some insects and plant groups), while those with good fossil records are somewhat neglected (e.g. foraminiferans, ostracods, bryozoans). In this contribution on cheilostome bryozoans, we present one of the largest species-level molecular phylogenies for any order of marine invertebrates, to alleviate the lack of molecular phylogenetic hypotheses for fossil-rich groups, and to answer long-standing evolutionary questions on timing and rates.

Members of the colonial Phylum Bryozoa have had important roles as marine ecosystem constructors and ecological interactors since their origins (*5*–*7*). They are long known to have an evolutionary history visible in the fossil record since the Early Ordovician (*8*) that has very recently been extended to the Cambrian (*9*). The constituent clades of Bryozoa have waxed and waned over geological time, with three classes, Phylactolaemata, Stenolaemata and Gymnolaemata still extant today (Fig. 1). The latter two classes are largely marine and calcified, and hence have rich fossil records. The order Cheilostomata within the Gymnolaemata have especially intricate skeletal morphologies that allow species-level delimitation, as shown using breeding experiments and allelic analyses (*10*). This suggests that cheilostome fossils are amenable to species-level identifications, an advantage for

integrating data from molecular sequences with fossil remains in order to reconstruct macroevolutionary history and processes. Cheilostomes are also the most species-rich order within Bryozoa with more than 6000 described extant species, and likely about the same number yet to be formally described (*11*). They represent c. 80% of the phylum's living species diversity (*12*). Likewise, there are c. 7900 described fossil cheilostome species documented in a new data compilation, where this number is a considerable underestimate of true fossil richness, based on models that account for incomplete sampling in the fossil record (*13*). Their benthic, largely sessile and encrusting life-habit allows us to investigate spatial competition frozen in geological time (*14*) and their modular and polymorphic nature permits the estimation of key biological parameters, including fitness components (*15*) beyond ecological time scales. The combination of these traits, their abundant fossil record and new molecular data provided in this contribution will facilitate empirical work on linking evolutionary processes on shorter (microevolutionary) time scales with those that unfold on longer (macroevolutionary) time scales.

Here, we first present genome-skimmed molecular data from the mitochondrial genome (15 genes) and two nuclear rRNA genes (18s and 28s) for 395 newly sequenced cheilostome specimens. We then combine these sequences with published data (sequences from 340 specimens) to estimate the phylogenetic relationships among more than 500 species and 225 genera of cheilostomes, from the poles to the tropics and from the intertidal to the deep sea. This represents about 10% and 40 % of the described extant cheilostome species and genera, respectively. Using this largest molecular phylogeny, in terms of both taxon- and gene-sampling, for cheilostomes to date, we investigate evolutionary hypotheses pertaining to age and rates.

We employ bryozoan (phylactolaemate, ctenostome, and cyclostome) and bilaterian outgroups and 18 fossil-calibration points, and present a time-calibrated bryozoan tree, asking

how much of the early lineage leading to extant cheilostomes is currently "invisible" (i.e. not detected) in the fossil record and when Bryozoa might have originated. Then we ask when (and how often) parental care in the form of incubation (brooding) evolved in the history of cheilostome evolution. The transition from a non-brooded embryo resulting in a long-lived, planktotrophic larva, to a brooded embryo resulting in a short-lived, non-feeding larva, is hypothesized to have driven rapid speciation among cheilostomes displaying the brooding trait (*16*). It is thought that species with non-feeding larvae disperse much shorter distances than those with feeding larvae and are hence associated with lower amounts of gene flow and consequently a higher speciation probability. Using our new time-tree, we ask if there is evidence that species with non-feeding larvae (note that all cheilostomes that brood possess only non-feeding larvae) are associated with higher speciation rates across the cheilostome clade.

While highlighting the continued need for an increased effort in systematics based on morphology and sequence data and broader taxon-sampling for phylogenetic inference, we underscore that this work is a significant step towards establishing cheilostomes as a model macroevolutionary system.

## Results

### 3.1 The largest cheilostome molecular phylogeny to date

The four extant bryozoan groups (phylactolaemates, cyclostomes, ctenostomes and cheilostomes) each form well-supported clades (Fig. 1, see Discussion on ctenostomes). Our full (Fig. S1, based on all the cheilostome sequences included in this study) and trimmed molecular phylogenies (Fig. S2, a subset of the full phylogeny trimmed with criteria listed in the methods) are illustrated in an abbreviated form in Fig. 1, highlighting the main inferred, and extant, clades of cheilostomes. Our cheilostome phylogeny has a well-supported

backbone with seven highly supported (Bootstrap BS > 90%, Fig. 1) ancestral nodes that gave rise to the depicted, and again highly supported, extant cheilostome clades (A-G, Figs. 1 and S2), albeit with the exception of the ancestral node (BS 64%) that resulted in the fully supported *Conopeum* genus (clade B, Figs. 1 and S2). The overall mean BS support is also high, averaging at 88.94% per node (calculated based on Fig. S2 with 721 taxa). The seven branches that led to the extant monophyletic A to G clades (Fig. 1) do not match the currently available broad systematic framework of cheilostomes (*17*). Our inferred topology (see SM section 4) substantially filled out regions of the cheilostome tree (i.e. *Scruparia* to *Macropora*) where key evolutionary transitions, including parental care (and hence non-feeding larvae), are thought to have taken place (*16*, *18*, *19*). The metadata associated with our new sequences (N = 516, where 395 cheilostomes and 5 cyclostomes are associated with physical vouchers with museum accession numbers; and 116 cheilostomes and 1 ctenostome without, see section 5 in SM) are presented in Table S1; genes used for phylogenetic inferences tabulated in Table S2 (mean = 14 genes out of 17 genes for 854 taxa); and NCBI accession numbers for deposited sequences in Table S3.

Our inferred tree topology, based solely on molecular sequences, largely supports the phylogenetic coherence of morphological species and genus concepts used by bryozoan taxonomists (Figs. S1 and S2). For instance, three specimens of *Klugeflustra vanhoffeni* collected during two different expeditions in distinct locations and identified by three independent experts (Table S1) are found to be monophyletic with little to no genetic distance based on 13 to 15 genes (Table S2, Fig. S1A). In a genus-level example, *Steginoporella*, represented in the next-most-recent cheilostome molecular phylogeny by five species (*20*) is now represented by nine species: *Steginoporella* was, and still is, monophyletic. The genus *Microporella* is here inferred by molecular sequences to include *Diporula* and *Flustramorpha*. These latter genera have been recently synonymized with *Microporella*

168 based purely on morphological grounds (*21*, *22*), likewise for the reassignment of
169 *Fenestrulina joannae* to *Microporella* (*22*). In contrast, many cheilostome families are
170 polyphyletic. For instance, genera of the family Smittinidae (*17*) are scattered throughout
171 clade G. Likewise, the genera of Bugulidae are scattered throughout clade C (Figs. 1, S1, S2,
172 see also SM section 4).
173
174 **3.2 A fossil-calibrated bryozoan tree and deep origins of clades**
175 Our phylogeny, fossil-calibrated on 18 nodes with a relaxed independent rates molecular
176 clock model (Fig. 2, see details of calibrations in Table S4 and SM text, joint time priors in
177 Fig. S3) suggests that bryozoans originated (i.e. became distinct from other Lophotrochozoa)
178 about 518 Mya (million years ago) (node iii, Fig. 2). This is the median value of the posterior
179 distribution with 95% Highest Posterior Density (HPD) between 495–547 Mya, i.e.
180 bryozoans are inferred to have originated in the Cambrian or as early as the Ediacaran (SM
181 Fig. S4 for sensitivity analyses using different clock models and calibrations). The node iv in
182 Fig. 2, where cyclostomes, and ctenostomes plus cheilostomes diverged from their common
183 ancestor shared with extant phylactolamates is estimated at 488 (HPD 471–517) Mya, i.e.
184 Late Cambrian or Early Ordovician. Node v, the divergence of cheilostomes plus
185 ctenostomes from other bryozoans is estimated at 407 (HPD 353–457) Mya, i.e. Early
186 Devonian. The cheilostome lineage is inferred to have diverged from ancestors shared with
187 ctenostomes in the Carboniferous (345 Mya, HPD 292–398 Mya), c. 200 million years earlier
188 than the confirmed fossil record of cheilostomes in the Late Jurassic (node vi, Fig. 2, see SM
189 Fig. S4 for sensitivity analyses). Two of the seven deep splits within the cheilostome clade
190 (nodes A, B in Fig. 1) are inferred to have happened in the Carboniferous, one in the Triassic
191 (node C in Fig. 1) and four in the Jurassic (nodes D to G in Fig. 1), while many lineages
192 leading to extant genera originated in the Cretaceous or Paleogene (see Fig. 2).

### 3.3 Evolution of parental care and speciation rates of brooders

Parental care in a form of embryonic incubation (brooding for short hereon) of non-feeding larvae, internally (inside zooidal cavity or internal brood sacs) or with specially developed external structures (membranous brood sacs and skeletal brood chambers), has independently evolved c. 5 times according to an ancestral state reconstruction (*23*) given our cheilostome tree topology (Fig. 3, Fig. S5). The transitions to brooding (and hence non-feeding larvae) are inferred to have occurred as early as the Permian (transition 4, Fig. 3). The brooding state is inferred never to have transitioned back to non-brooding, while the non-brooding state transitions to a brooding state at a rate of 0.1888 per 100 million years (std err 0.0503).

Based on an information criterion-based comparison of Binary State Speciation and Extinction (BiSSE) (*24*), Hidden State Speciation and Extinction (HiSSE) models (*25*) and their null versions, we rejected a model where brooding is associated with differential rates of speciation. Here, a null BiSSE model (character independent model with two states, "cid2" see Methods section 2.8), has the highest AIC model weight (0.581) of the five models we compared (Table 1, see Table S6 for all parameter estimates). We also compared the same models with two alternative topologies, one where *Lunularia* is removed and one where *Conopeum* is alternatively placed as sister to all other cheilostomes (see methods and SM for reasoning). In both latter cases, we rejected a model where brooding is directly associated with differential rates of speciation, but found strong support for a model where unmeasured states associated with the brooding state drove higher speciation rates (see Table S7 for model weights).

## Discussion

Cheilostome bryozoans have exceptionally useful traits for tackling some long-standing questions in evolutionary biology. Such traits include a calcified skeleton that renders these

218 marine organisms very fossilizable (*7*), external, calcified brooding structures that allow
219 fecundity (a fitness component) to be quantified in the fossil record (*15*), a colonial and
220 modular nature that allows the estimation of sources of phenotypic variation among and
221 within individual genotypes and environments (*26*, *27*), polymorphic structures that represent
222 ergonomically partitioned divisions of labor (*28*, *29*), and ecological interactions "frozen in
223 time" (*6*, *14*). Analyzing molecular sequence data, independent of morphological traits used
224 to identify species, to infer evolutionary relationships, we lend strong support to important
225 assumptions often invoked in the cheilostome literature with limited empirical support. The
226 first is that skeletal traits can be used to identify cheilostome species (*10*), as separate
227 specimens identified as the same species (based only on morphology) have little genetic
228 distance in our inferred tree. The second is that cheilostome genera are natural groupings
229 (monophyletic or paraphyletic clades) and can arguably be used as unit of evolutionary
230 analysis (*30*, *31*). In addition, by generating a large volume of molecular sequences for
231 cheilostome species, we are primed for an integration of such data with their morphological
232 characters, moving one step closer to total-evidence analyses (*3*). Such a phylogeny will
233 allow us to answer other long-standing general evolutionary questions, including whether
234 higher rates of morphological evolution happen close to speciation events (*32*).
235 Age and rates are two major features of evolution and we contribute information with
236 regards to both. The phylum Bryozoa has been considered enigmatic not least because it is
237 the only potentially fossilizable metazoan phylum with no body-fossil representation in the
238 Cambrian record (*33*), until very recently (*9*). Our main analysis and our sensitivity analyses
239 with alternative calibration and clock assumptions (Fig. S4) have inferred Bryozoa to have
240 originated in the Cambrian, an idea first proposed by Hyman (1959), or even as early as the
241 late Ediacaran, despite the lack of fossil remains (see SM for a discussion of *Pywakia,* a
242 controversial Cambrian fossil). The lineage ancestral to living cheilostomes and ctenostomes

has two peaks in its posterior age distribution (node v, Fig. 2), where the older peak overlaps the calibration and the younger peak does not. This may be an artifact of using boring ctenostomes as a calibration point, while our molecular data are represented by perhaps very distantly related, non-boring ctenostomes, i.e. there is a conflict between the fossil calibration and the molecular data for this node. This can be resolved by including boring ctenostomes in the phylogeny, although extracting sequences given their life habit is currently challenging.

The cheilostome fossil record is long and rich (*35*), and we might have expected cheilostome origins to be on the order of only a few tens of million years earlier than the oldest cheilostome fossil from the Late Jurassic (*36*). However, given the tree topology, gene-sampling and multiple fossil calibrations and sensitivity analyses (Fig. S4), we have estimated the evolutionary origin of cheilostomes to be Paleozoic, somewhat earlier than the only other study based on sequence data to estimate cheilostome origins (*37*). Hao *et al.* (2005) estimated cheilostomes to have originated in the Permian to the Early Triassic, based on only one nuclear gene (16S), 40 taxa and one calibration point, which we did not include as we did not have sequences pertaining to that node. While one might postulate that extinct bryozoan groups that are contemporary with this "invisible" stem-lineage could be possible cheilostome progenitors, we currently have no clear candidates that we can reasonably suggest from the fossil record (*7*). Both our tree topology and our understanding of their morphology points to the gymnolaemate order Ctenostomata as the most likely ancestor for crown-group Cheilostomata. However, ctenostomes are known only from borings in the Paleozoic and there are only a few fossils of ctenostomes, even in the more recent fossil record (*38*). This hints at largely uncalcified stem and ancestral crown cheilostome lineages (e.g. calcified skeletons in crown group cheilostomes may have multiple origins), and/or perhaps encrusting, calcified taxa favoring substrates that do not easily preserve. It is plausible that increasing taxon-sampling and/or applying more complex models that allow for

total-evidence analyses could help us refine this and other age estimates in our bryozoan tree (*39*), but data for such analyses are not yet available. Interestingly, four of the seven deep branches emerging from the backbone (Fig. 1) emerged throughout the Jurassic, at the end of which the fossil record of cheilostomes began with a trickle. Similarly, many lineages leading to extant genera are inferred to have originated in the Cretaceous (Fig. 2), when the fossil record of cheilostomes exploded in its morphological disparity and observed abundance. This suggests that when cheilostomes lineages are observed in the fossil record, they are likely to have been extant for a substantial amount of time, perhaps at lower abundances or in cryptic habitats that enter the fossil record at a much lower rate. The continued exploration of the fossil record of bryozoans may yet reveal surprises, as even originations of groups as well-studied as land plants continue to astonish (*40*) and the relationships among metazoan groups remain elusive (*41*).

A planktotrophic larva, associated with a non-brooding state, is found to be the ancestral condition in cheilostomes, based on the topology of our inferred tree, as long hypothesized in the literature (*19*, *34*). This is despite the living members of ctenostomes (putative ancestors of cheilostomes) displaying varied levels of parental care, ranging from planktotrophic larvae to complex forms of embryonic incubation (*42*, *43*).

Parental care is thought to not only confer fitness advantages (*44*) but in the case of cheilostomes it is also hypothesized to be associated with increased speciation rates (*16*). The given reason is the association of brooding with non-feeding larvae that are unable to survive in the water column for extended periods of time and that hence settle close to their parental colonies. The evolutionary reversal of non-feeding back to feeding larvae is thought to be uncommon among marine invertebrates (*45*) and we have shown here for cheilostomes that this is true: feeding larvae, once lost, never re-evolved. Although brooding and non-feeding larvae are “irreversibly” evolved very early in their history, the apparent higher speciation

293 rates of cheilostomes that brood are unlikely due (directly) to the brooding/non-feeding
294 larvae. This is in contrast to other empirical studies based on different taxa, that suggest larva
295 dispersal modes or geographic range sizes associated with them directly influencing
296 diversification rates (*46*). Rather, it could be "external" factors, such as the
297 macroevolutionary influence from a competing clade, the cyclostomes, that drove their
298 diversification (*13*) as suggested by a character-independent model of speciation and
299 extinction (Table 1). Alternatively, an unmeasured trait that is associated with brooding/non-
300 feeding larvae, could be responsible for differential rates of diversification in cheilostomes
301 (Table S7). One such trait could be increased polymorphism. For example, spines, considered
302 as modified polymorphic zooids, can (evolutionarily) develop into brood chambers or frontal
303 shields, i.e. morphological structures with functions different from the original ones (*29*). A
304 diversity of traits, derived from polymorphs in a modular construction, that permit varied or
305 even novel ecological function, could allow the occupation of new niches and thus promote
306 macroevolutionary diversification (*28*).
307 Phylogenetic topologies and inferences made from them are limited by both taxon and
308 gene sampling (*47*, *48*). Although our phylogeny is the largest in terms of both taxon and
309 gene sampling for cheilostome bryozoans, the inferences presented here are far from final.
310 However, our data are the seed for new data accumulation and our inferred tree a starting
311 point for many more sophisticated macroevolutionary analyses. Our estimated node ages are
312 subject to the well-known and well-studied limitations of the molecular clock (*49*), our
313 knowledge of the evolution of the group and its fossil record. The ancestral state
314 reconstructions we performed did not incorporate trait information from fossil taxa, whose
315 inclusion would most definitely improve such analyses (*50*). While Hidden State Speciation
316 and Extinction Rate models (*25*) overcomes some statistical issues inherent in earlier related
317 models (*51*), extinction rates estimated from phylogenies based only on extant taxa are still

non-ideal and also limit the interpretation of our analyses (*24*, *25*), even though we focused on trait and speciation rate estimation. Despite the limitations listed, this largest cheilostome tree to date has provided first glimpses of the timing and tempo of evolution of main clades and a key trait for an ecologically and evolutionarily important order that has been overlooked for too long.

This work emphasizes that continued collaborative research between molecular phylogeneticists, systematists, paleontologists and macroevolutionary biologists can confirm and elucidate relationships, identify important gaps, understand timing and rates of evolution and open a window into evolution itself, even before integrating substantial data from the fossil record.

## Methods

### *2.1. Sampling and taxon identification*

The procedure summarized from Sections 2.1 to 2.5 follows (*20*) closely with minimum modifications. Colonies whose sequences are presented here were collected and preserved in 70-96% ethanol (Table S1). Each colony, preliminarily identified to the lowest possible taxonomic level using a stereoscope, was subsampled for DNA isolation and scanning electron microscopy. While we aimed at sequencing a colony for each distinct species, uncertainty in initial taxon identification using a stereoscope combined with a realization that within-taxon replicates are important for sequence verification, compelled us to include such replicates. The scanning electron micrographs (see SEM cards deposited in Zenodo https://zenodo.org/record/5721078#.YZz39VMo_fY), taken with a Hitachi TM4040PLus after bleaching to remove tissue where appropriate, are required for species-level identification and serve as digital vouchers, in addition to physical vouchers deposited at the Natural History Museum in Oslo (Table S1). Taxonomic identifications were made

343 independently of, but are subsequently verified using the phylogenetic inference and
344 metadata.
345 Due to the microscopic nature of cheilostomes and their benthic and often encrusting
346 lifestyle, each visible colony (see paragraph above) is often a mixed tissue sample that could
347 consist of other organisms including non-target cheilostome species. Rather than treating
348 non-target species as contaminants to be discarded, we leverage these to lend clarity to the
349 cheilostome phylogeny (Fig. S1). There are three classes of non-target specimens. The first is
350 where we have found enough macroscopic remains of the non-target cheilostome, post-
351 sequencing, for imaging. In the second class, we did not find any remaining macroscopic
352 material but given our taxon sampling and observed sequences, we are certain that the
353 contaminant belongs to a given taxon (these are labeled with taxon names and "SEQ" in Fig.
354 S1). In yet other cases, given the tree topology and observed sequences, we do not assign the
355 unvouchered sequences to any known taxon name (these are labelled "UNKNOWN" in Fig.
356 S1, see SM for criteria and examples of all three types of non-target sequences and Table S1
357 for their metadata).
358
359 ***2.2. DNA isolation, sequencing and assembly***
360 The subsamples of colonies (henceforth "samples") were dried before genomic DNA
361 isolation using the DNeasy Blood and Tissue kit (QIAGEN, Germantown, MD, USA).
362 Samples were homogenized with a pestle in lysis buffer, in the presence of proteinase-K.
363 Genomic DNA were sequenced at the Norwegian Sequencing Centre (Oslo, Norway) using
364 Illumina HiSeq4000 150 bp paired-end (PE) sequencing with a 350 bp insert size.
365 Approximately 20 samples were genome-skimmed (multiplexed) on a single lane. Illumina
366 HiSeq reads were quality checked using FastQC v.0.11.8 (*52*) , then quality- and adapter-
367 trimmed using TrimGalore v0.4.4 with a Phred score cutoff of 30 (*53*). Trimmed reads were

*de novo* assembled with SPAdes 3.13 (*54*) using k-mers of 21, 33, 55, 77, 99 and 127. The mitogenome and rRNA operon of each sample were identified separately with blastn (*55*) using blast+ against a database constructed from cheilostome sequences available in NCBI (*20*). An E-value of 1.00e-185 and maximum target sequence of 1 were used to filter any blast hits of non-cheilostome origin.

### *2.3. Annotation*

Mitogenomes for each of the samples were annotated with Mitos2 using a metazoan reference (RefSeq 89) and the invertebrate genetic code (*56*) to identify two rRNA (rrnL and rrnS) and 13 protein coding genes (*atp6, atp8, cox1, cox2, cox3, cob, nad1, nad2, nad3, nad4, nad4l, nad5,* and *nad6*). Two nuclear rRNA operon genes (ssu/18s and lsu/28s) were also identified and annotated using RNAmmer (*57*). 315 published cheilostome sequences (*20*, *58–60*) and the mitogenomes and rRNA operons of 31 non-cheilostome outgroup taxa, both bryozoan and non-bryozoan, were aligned with our sequences to compile a broader outgroup taxon sample (Table S3).

### *2.4. Sequence alignment*

MAFFT (*61*) was used for alignment with default parameters: for the four rRNA genes (nucleotide) the Q-INS-i model, considering secondary RNA structure, was utilized; for the 13 protein-coding genes, in amino acid format, the G-INS-I model was used. The 17 separate alignments were edited manually using Mesquite v3.61 to remove any uncertain characters (*62*). Ambiguously aligned characters were removed from each alignment using Gblocks (*63*) with least stringent parameters. The single-gene alignments were concatenated to a supermatrix using the catfasta2phyml perl script (*64*). The alignments (both masked and unmasked) will be available through Dryad (https://doi.org/10.5061/dryad.2v6wwpzp9)

Access for reviewers is currently available here:

https://datadryad.org/stash/share/N0OEY8a339xu2E0g2X4Eirzb--OwL7s6uZaJ0AMnQ70

### *2.5. Datasets for phylogenetic reconstruction*

As mentioned in section 2.1, cheilostomes are small and attached to substrata so even the most macroscopically pristine sample may have sequences of non-target species included. Where the contaminants are non-cheilostome, they are removed bioinformatically (see section 2.2). Here, we utilize the non-target cheilostome sequences (see also 2.1). As such, two concatenated datasets are presented: 1) "Full alignment" is the alignment with our largest taxon sample. It includes both "UNKNOWN" (cheilostomes lacking both a voucher (physical and/or SEM) and an inferred taxonomic identity) and "SEQ" (cheilostomes lacking a voucher (SEM) but with an inferred taxonomic identity), constructed to show the hidden diversity within the phylum (Fig. S1). "Full alignment" also includes cheilostomes previously sequenced and available from NCBI and non-cheilostome and non-bryozoan outgroups (Table S2). 2) "Trimmed alignment" is the alignment where "UNKNOWN", "SEQ", and those taxa with less than three genes and "rogue taxa" are pruned using RogueNaRok (*65*). We picked a three-gene cut off after preliminary analyses showed that this is the best compromise between the number of taxa included and bootstrap support for our tree inference. "Rogue taxa" are those with unstable phylogenetic affinities based on evaluation of the extended majority-rule consensus (MRE) threshold, optimized for support and with a maximum dropset size of 1. Those with a sum >0.2 were pruned from the "trimmed alignment" dataset. Note that the ML tree topologies are respectively termed "Full tree" and "Trimmed tree" from the full alignment and trimmed alignment datasets respectively. For each of the two datasets, ambiguously aligned characters were removed from each single gene alignment using Gblocks (*63*) with least stringent parameters prior to concatenation.

### *2.6. Phylogenetic reconstruction and congruence test*

Maximum likelihood (ML) phylogenetic analyses were carried out for each single gene alignment using the "AUTO" parameter in RAxML v8.0.26 (*66*) to establish the evolutionary model with the best fit. The general time reversible (GTR+G) was the preferred model for the four rRNA genes (18s, 28s, rrnS and rrnL), and MtZoa+G for all 13 protein coding genes. The two concatenated datasets (see section 2.5) were divided into four separate rRNA and 13 protein gene partitions each (17 partitions in total) with its own distinct gamma distribution to accommodate for different substitution patterns among sites, and were analyzed using RAxML. For comparison, a partitioning scheme based on AICc and a greedy search scheme suggested by PartitionFinder2 (*67*) was also analyzed using RAxML. The topology with the highest likelihood score of 100 heuristic searches was chosen and bootstrap values were calculated from 500 pseudo-replicates. As the first partition scheme (17 partitions) gave a higher likelihood score, we present the topology based on that, rather than the one suggested by PartitionFinder2. Bootstrap values presented were calculated from 500 pseudo-replicates.

The topology of the phylogenetic tree in this contribution was compared to that from (*20*) to gauge if a substantial increase in sampled taxa had any detectable bearing on the inferred topology. To this end we trimmed samples not represented in (*20*) from the full tree (Fig. S1) and using Dendroscope (*68*) compared the topology of their remaining 263 shared taxa using the $I_{cong}$ index (*69*).

### *2.7. Fossil-calibration and Bayesian divergence time estimation*

We use MCMCTree v4.9 (*70*) for divergence time estimation as it allows us to analyze amino acid and nucleotide partitions simultaneously and takes relatively less computational power than other comparable software. As input to MCMCTree, we use the trimmed tree (Fig. S2),

443 but to reduce computational burden further we removed the following taxa: (i) those lacking
444 species and/or genus designations and those assigned “cf. and aff.”; and (ii) species
445 duplicates with the largest number of alignment gaps. If a genus is represented by multiple
446 species, a maximum of three different named species were retained, choosing those with the
447 least number of alignment gaps. Note that this dataset was created before minor changes
448 detailed in the SM (section 4). Excluded taxa were deleted from the amino acid and
449 nucleotide alignments, whilst corresponding leaves for the same taxa were removed using
450 Dendroscope (*68*) thus maintaining the topological branching pattern of the original rooted
451 input tree (Fig. S2). The resulting dataset consisted of 363 taxa where 335 are cheilostomes.

452 We applied a hard upper limit of 636 Mya to the root, representing the bilaterian
453 maximum (*71*, *72*). We used 18 internal fossil calibrated nodes (see Table S4 and Fig. S3 for
454 details). To explore the impact of calibration prior choice we ran different sets of analyses: (i)
455 “L”, with minimum constraints only (Table S4), using the truncated Cauchy distribution with
456 a soft minimum and a diffuse tail; (ii) “B”, with uniform constraints with soft minimum and
457 maximum bounds corresponding to the fossil ages; (iii) “ST”, with a skew-T distribution such
458 that the 1% and 99% probability tails correspond to the minimum and maximum constraints
459 (Table S4). In all cases we always used “soft bound” where there is a 1% chance that a node
460 could be younger or older than the specified constraints. Upon examining initial results for
461 “B” and “ST”, we find that we had to impose a hard minimum constrain within our outgroup
462 on the Pancrustacea node, otherwise we recovered an unreasonably young posterior
463 distributions (although we note this does not affect the ages recovered for the ingroup nodes,
464 see Fig. S4). We hence also present the “B” and “ST” analyses with a hard constraint on the
465 Pancrustacea node only (“BL” and “STL”, respectively). For all five sets of analyses (B, BL,
466 L, ST, STL), we ran both independent and autocorrelated molecular clock models. The main
467 results we present use the independent clock model and “STL”, as branches close to the root

of the tree represent huge evolutionary distances and because it seems logical to put prior weight around the ages of the fossil calibrations since the fossil record of cheilostomes is considered excellent. Mixing was checked by inspecting the trace plots and ensuring the effective sample sizes were greater than 200 for all node ages and model parameters. In addition, we ensured that independent chains converged on the same values. For details of the substitution model, MCMC settings see the SM section 3 "MCMCtree settings".

### *2.8. Ancestral state reconstruction and HiSSE*

Data for non-brooding species with planktotrophic larvae (state = 0) and brooding species with non-feeding larvae (state = 1) of all the cheilostomes species included in the calibration tree (N = 335), are provided in Table S5. To estimate brooding states of the internal nodes, we use a standard Markov model of binary character evolution (*23*) implemented in ape (*73*), where a maximum likelihood joint estimation procedure was performed. Note that although the tree for the analyses described in this section is pruned, the non-brooding/brooding states we are concerned are conserved at genus-level. To detect possible differences in diversification rates associated with the non-brooding or brooding state, we applied trait-dependent speciation and extinction models (SSE) implemented in the R package HiSSE (*25*) to the fossil calibrated tree (N= 355) where we used the STL calibration with an independent clock model (see section 2.7). We estimate that we have sampled 0.7% and 9.5% of species of non-brooders and brooders (*17*), respectively, in our calibration tree and use this as information to account for biases due to incomplete sampling. We ran three different null models ("null", "cid2" and "cid4"), a binary state speciation and extinction model (BiSSE) and a hidden state speciation and extinction model (HiSSE) to investigate if brooding might be associated with higher speciation rates. The "null" constrains speciation and extinction to be equal regardless of brooding state. A BiSSE model allows speciation and extinction to be different for the non-brooding versus brooding state. The first character-independent model

493 ("cid2") allows two different sets of speciation and extinction to be estimated but does not
494 link these to the observed traits, such that it has the same level of complexity as the null
495 version of the BiSSE model. A HiSSE model assumes that there are unmeasured states that
496 display distinct rates of speciation and extinction but that these states are associated with the
497 coded state. In other words, HiSSE allows for the scenario in which a state co-associated with
498 brooding drives the differences between the observed differences in speciation among species
499 with and without brooding. The second character-independent model ("cid4") allows four
500 different sets of speciation and extinction, such that the model has the same level of
501 complexity as a HiSSE model and serves as its null model. The five models are compared
502 using AIC model weights and their parameter estimates also presented.
503 Because the topological placement of *Lunularia* is starkly incongruent with
504 morphology as we understand it (see SM), we also compared the same five models with a
505 time-tree where *Lunularia* is removed. Additionally, as the BS support for *Conopeum* is
506 weaker than for other major nodes in our tree and because it is a key taxon, we again
507 compared the same models but using an alternative topology where *Conopeum* is placed as
508 sister to all other cheilostomes.
509
510 **References cited in main text and SM**

511 1. R. M. D. Beck, C. Baillie, Improvements in the fossil record may largely resolve
512 current conflicts between morphological and molecular estimates of mammal
513 phylogeny. *Proc. R. Soc. B-Biological Sci.* **285**, 20181632 (2018).
514 2. N. M. Koch, L. A. Parry, Death is on our side: paleontological data drastically modify
515 phylogenetic hypotheses. *Syst. Biol.* **69**, 1052–1067 (2020).
516 3. F. Ronquist, S. Klopfstein, L. Vilhelmsen, S. Schulmeister, D. L. Murray, A. P.
517 Rasnitsyn, A total-evidence approach to dating with fossils, applied to the early

radiation of the Hymenoptera. *Syst. Biol.* **61**, 973–999 (2012).

4. D. W. Bapst, H. A. Schreiber, S. J. Carlson, Combined analysis of extant Rhynchonellida (Brachiopoda) using morphological and molecular data. *Syst. Biol.* **67**, 32–48 (2018).

5. A. C. L. Wood, P. K. Probert, A. A. Rowden, A. M. Smith, Complex habitat generated by marine bryozoans: a review of its distribution, structure, diversity, threats and conservation. *Aquat. Conserv. Mar. Freshw. Ecosyst.* **22**, 547–563 (2012).

6. P. D. Taylor, M. A. Wilson, Palaeoecology and evolution of marine hard substrate communities. *Earth-Science Rev.* **62**, 1–103 (2003).

7. P. D. Taylor, *Bryozoan Paleobiology* (Wiley-Blackwell, 2020).

8. F.-S. Xia, S.-G. Zhang, Z.-Z. Wang, The oldest bryozoans: new evidence from the Late Tremadocian (Early Ordovician) of East Yangtze Gorges in China. *J. Paleontol.* **81**, 1308–1326 (2007).

9. Z. Zhang, Z. Zhang, J. Ma, P. D. Taylor, L. C. Strotz, S. M. Jacquet, C. B. Skovsted, F. Chen, J. Han, G. A. Brock, Fossil evidence unveils an early Cambrian origin for Bryozoa. *Nature*. **599**, 251–255 (2021).

10. J. B. C. Jackson, A. H. Cheetham, Evolutionary significance of morphospecies - a test with cheilostome Bryozoa. *Science.* **248**, 579–583 (1990).

11. D. P. Gordon, M. J. Costello, Bryozoa – not a minor phylum. *New Zeal. Sci. Rev. 73(3-4)*. **73**, 63–66 (2016).

12. P. E. Bock, D. Gordon, Phylum Bryozoa Ehrenberg, 1831. *Zootaxa*. **3703**, 67–74 (2013).

13. S. Lidgard, E. Di Martino, K. Zagorsek, L. H. Liow, When fossil clades ‘compete’: local dominance, global diversification dynamics and causation. *Proc. R. Soc. B-Biological Sci.* **288**, 20211632 (2021).

14. L. H. Liow, E. Di Martino, G. Krzeminska, M. Ramsfjell, S. Rust, P. D. Taylor, K. L. Voje, Relative size predicts competitive outcome through 2 million years. *Ecol. Lett.* **20**, 981–988 (2017).
15. E. Di Martino, L. H. Liow, Trait-fitness associations do not predict within-species phenotypic evolution over 2 million years. *Proc. R. Soc. B-Biological Sci.* **288**, 20202047 (2021).
16. P. D. Taylor, Major radiation of cheilostome bryozoans: trigger by the evolution of a new larval type? *Hist. Biol.* **1**, 45–64 (1988).
17. P. E. Bock, Indexes to Bryozoan Taxa. (2021), (available at http://www.bryozoa.net/).
18. D. Jablonski, S. Lidgard, P. D. Taylor, Comparative ecology of bryozoan radiations: origin of novelties in cyclostomes and cheilostomes. *Palaios*. **12**, 505–523 (1997).
19. A. N. Ostrovsky, *Evolution of Sexual Reproduction in Marine Invertebrates* (Springer, Dordrecht Heidelberg New York London, 2013).
20. R. J. S. Orr, E. Di Martino, D. P. Gordon, M. H. Ramsfjell, H. L. Mello, A. M. Smith, L. H. Liow, A broadly resolved molecular phylogeny of New Zealand cheilostome bryozoans as a framework for hypotheses of morphological evolution. *Mol. Phylogenet. Evol.* **161**, 107172 (2021).
21. E. Di Martino, P. D. Taylor, D. P. Gordon, Erect bifoliate species of *Microporella* (Bryozoa, Cheilostomata), fossil and modern. *Eur. J. Taxon.* **679**, 1–31 (2020).
22. E. Di Martino, A. Rosso, Seek and ye shall find: new species and new records of *Microporella* (Bryozoa, Cheilostomatida) in the Mediterranean. *Zookeys*. **1053**, 1–42 (2021).
23. M. Pagel, Detecting correlated evolution on phylogenies: a general method for the comparative analysis of discrete characters. *Proc. R. Soc. B-Biological Sci.* **255**, 37–45 (1994).

568 24. W. P. Maddison, P. E. Midford, S. P. Otto, Estimating a binary character's effect on
569 speciation and extinction. *Syst Biol*. **56**, 701–710 (2007).
570 25. J. M. Beaulieu, B. C. O'Meara, Detecting hidden diversification shifts in models of
571 trait-dependent speciation and extinction. *Syst. Biol.* **65**, 583–601 (2016).
572 26. A. H. Cheetham, J. B. C. Jackson, L. A. C. Hayek, Quantitative genetics of bryozoan
573 phenotypic evoluion. 1. rate tests for random change versus selection in differentiation
574 of living species. *Evolution.* **47**, 1526–1538 (1993).
575 27. A. H. Cheetham, J. B. C. Jackson, L. A. C. Hayek, Quantitative genetics of bryozoan
576 phenotypic evolution. 2. Analysis of selection and random change in fossil species
577 using reconstructed genetic-parameters. *Evolution.* **48**, 360–375 (1994).
578 28. C. R. Schack, D. P. Gordon, K. G. Ryan, Modularity is the mother of invention: a
579 review of polymorphism in bryozoans. *Biol. Rev.* **94**, 773–809 (2019).
580 29. S. Lidgard, M. C. Carter, M. H. Dick, D. P. Gordon, A. N. Ostrovsky, Division of
581 labor and recurrent evolution of polymorphisms in a group of colonial animals. *Evol.*
582 *Ecol.* **26**, 233–257 (2012).
583 30. A. M. Humphreys, T. G. Barraclough, The evolutionary reality of higher taxa in
584 mammals. *Proc. R. Soc. B-Biological Sci.* **281** (2014).
585 31. J. R. Hendricks, E. E. Saupe, C. E. Myers, E. J. Hermsen, W. D. Allmon, The
586 generification of the fossil record. *Paleobiology*. **40**, 511–528 (2014).
587 32. N. Eldredge, S. J. Gould, in *Models in Paleobiology* , T. J. M. Schopf, Ed. (W.H.
588 Freeman & Company, 1972), pp. 82–115.
589 33. J. W. Valentine, D. H. Erwin, D. Jablonski, Developmental evolution of metazoan
590 bodyplans: the fossil evidence. *Dev. Biol.* **173**, 373–381 (1996).
591 34. L. H. Hyman, *The invertebrates: smaller coelomate groups* (McGraw-Hill, New York,
592 1959).

593 35. F. K. McKinney, S. Lidgard, J. J. Sepkoski, P. D. T. Taylor, Decoupled temporal
594 patterns of evolution and ecology in two post-Paleozoic clades. *Science.* **281**, 807–809
595 (1998).
596 36. P. D. Taylor, An early cheilostome bryozoan from the Upper Jurassic of Yemen.
597 *Neues Jahrb. für Geol. und Paläontologie Abhandlungen*. **191**, 331–344 (1994).
598 37. J. Hao, C. Li, X. Sun, Q. Yang, Phylogeny and divergence time estimation of
599 cheilostome bryozoans based on mitochodrial 16S rRNA sequences. *Chinese Sci. Bull.*
600 **50**, 1205–1211 (2005).
601 38. P. D. Taylor, Bioimmured ctenostomes from the Jurassic and the origin of the
602 cheilostome Bryozoa. *Palaeontology*. **33**, 19–34 (1990).
603 39. A. Gavryushkina, T. A. Heath, D. T. Ksepka, T. Stadler, D. Welch, A. J. Drummond,
604 Bayesian total-evidence dating reveals the recent crown radiation of penguins. *Syst.*
605 *Biol.* **66**, 57–73 (2017).
606 40. P. K. Strother, C. Foster, A fossil record of land plant origins from charophyte algae.
607 *Science.* **373**, 792–796 (2021).
608 41. C. E. Laumer, R. Fernandez, S. Lemer, D. Combosch, K. M. Kocots, A. Riesgo, S. C.
609 S. Andrade, W. Sterrer, M. Sorensen V, G. Giribet, Revisiting metazoan phylogeny
610 with genomic sampling of all phyla. *Proc. R. Soc. B-Biological Sci.* **286** (2019),
611 doi:10.1098/rspb.2019.0831.
612 42. A. N. Ostrovsky, D. P. Gordon, S. Lidgard, Independent evolution of matrotrophy in
613 the major classes of Bryozoa: transitions among reproductive patterns and their
614 ecological background. *Mar. Ecol. Prog. Ser.* **378**, 113–124 (2009).
615 43. R. Ström, in *Biology of Bryozoans.*, R. M. Woollacott, R. L. Zimmer, Eds. (Academic
616 Press, New York, 1977), p. 23–55.
617 44. S. C. Stearns, Trade-offs in life-history evolution. *Funct. Ecol.* **3**, 259–268 (1989).

618 45. R. R. Strathmann, The evolution and loss of feeding larval stages of marine
619 invertebrates. *Evolution.* **32**, 894–906 (1978).
620 46. D. Jablonski, G. Hunt, Larval ecology, geographic range, and species survivorship in
621 Cretaceous mollusks: Organismic versus species-level explanations. *Am. Nat.* **168**,
622 556–564 (2006).
623 47. T. A. Heath, D. J. Zwickl, J. Kim, D. M. Hillis, Taxon sampling affects inferences of
624 macroevolutionary processes from phylogenetic trees. *Syst. Biol.* **57**, 160–166 (2008).
625 48. R. A. Pyron, Post-molecular systematics and the future of phylogenetics. *Trends Ecol.*
626 *Evol.* **30**, 384–389 (2015).
627 49. F. Rodríguez-Trelles, R. Tarrío, F. J. Ayala, A methodological bias toward
628 overestimation of molecular evolutionary time scales. *Proc. Natl. Acad. Sci.* **99**, 8112–
629 8115 (2002).
630 50. J. A. Finarelli, J. J. Flynn, Ancestral state reconstruction of body size in the Caniformia
631 (Carnivora, Mammalia): The effects of incorporating data from the fossil record. *Syst.*
632 *Biol.* **55**, 301–313 (2006).
633 51. D. L. Rabosky, E. E. Goldberg, Model inadequacy and mistaken inferences of trait-
634 dependent speciation. *Syst. Biol.* **64**, 340–355 (2015).
635 52. S. Andrews, FastQC: A quality control tool for high throughput sequence data.
636 Available online at: http://www.bioinformatics.babraham.ac.uk/projects/fastqc/ (2010).
637 53. F. Krueger, TrimGalore. (2015), (available at
638 https://www.bioinformatics.babraham.ac.uk/projects/trim_galore/).
639 54. A. Bankevich, S. Nurk, D. Antipov, A. A. Gurevich, M. Dvorkin, A. S. Kulikov, V. M.
640 Lesin, S. I. Nikolenko, S. Pham, A. D. Prjibelski, A. V Pyshkin, A. V Sirotkin, N.
641 Vyahhi, G. Tesler, M. A. Alekseyev, P. A. Pevzner, SPAdes: a new genome assembly
642 algorithm and its applications to single-cell sequencing. *J. Comput. Biol.* **19**, 455–477

(2012).

55. S. F. Altschul, W. Gish, W. Miller, E. W. Myers, D. J. Lipman, Basic local alignment search tool. *J. Mol. Biol.* **215**, 403–410 (1990).

56. M. Bernt, A. Donath, F. Jühling, F. Externbrink, C. Florentz, G. Fritzsch, J. Pütz, M. Middendorf, P. F. Stadler, MITOS: Improved *de novo* metazoan mitochondria genome annotation. *Mol. Phylogenet. Evol.* **69**, 313–319 (2013).

57. K. Lagesen, P. Hallin, E. A. Rødland, H.-H. Staerfeldt, T. Rognes, D. W. Ussery, RNAmmer: consistent and rapid annotation of ribosomal RNA genes. *Nucleic Acids Res.* **35**, 3100–3108 (2007).

58. R. J. S. Orr, M. N. Haugen, B. Berning, P. Bock, R. L. Cumming, W. K. Florence, M. Hirose, E. Di Martino, M. H. Ramsfjell, M. M. Sannum, A. M. Smith, L. M. Vieira, A. Waeschenbach, L. H. Liow, A genome-skimmed phylogeny of a widespread bryozoan family, Adeonidae. *BMC Evol. Biol.* **19**, 235 (2019).

59. R. J. S. Orr, M. M. Sannum, S. Boessenkool, E. Di Martino, D. P. Gordon, H. L. Mello, M. Obst, M. H. Ramsfjell, A. M. Smith, L. H. Liow, A molecular phylogeny of historical and contemporary specimens of an under-studied micro-invertebrate group. *Ecol. Evol.* **11**, 309– 320 (2020).

60. R. J. S. Orr, A. Waeschenbach, E. L. G. Enevoldsen, J. P. Boeve, M. N. Haugen, K. L. Voje, J. Porter, K. Zágoršek, A. M. Smith, D. P. Gordon, L. H. Liow, Bryozoan genera *Fenestrulina* and *Microporella* no longer confamilial; multi-gene phylogeny supports separation. *Zool. J. Linn. Soc.*, zly055–zly055 (2018).

61. K. Katoh, D. M. Standley, MAFFT Multiple equence Alignment Software Version 7: Improvements in performance and usability. *Mol. Biol. Evol.* **30**, 772–780 (2013).

62. W. P. Maddison, D. R. Maddison, Mesquite: a modular system for evolutionary analysis. Version 3.1 (2017), (available at http://mesquiteproject.org).

668 63. G. Talavera, J. Castresana, Improvement of phylogenies after removing divergent and
669 ambiguously aligned blocks from protein sequence alignments. *Syst Biol*. **56**, 564–577
670 (2007).
671 64. J. A. A. Nylander, catfasta2phyml. (2010), (available at
672 https://github.com/nylander/catfasta2phyml).
673 65. A. J. Aberer, D. Krompass, A. Stamatakis, Pruning rogue taxa improves phylogenetic
674 accuracy: an efficient slgorithm and webservice. *Syst. Biol.* **62**, 162–166 (2013).
675 66. A. Stamatakis, RAxML-VI-HPC: maximum likelihood-based phylogenetic analyses
676 with thousands of taxa and mixed models. *Bioinformatics*. **22**, 2688–2690 (2006).
677 67. R. Lanfear, P. B. Frandsen, A. M. Wright, T. Senfeld, B. Calcott, PartitionFinder 2:
678 New methods for selecting partitioned models of evolution for molecular and
679 morphological phylogenetic analyses. *Mol. Biol. Evol.* **34**, 772–773 (2017).
680 68. D. H. Huson, C. Scornavacca, Dendroscope 3: an interactive tool for rooted
681 phylogenetic trees and networks. *Syst. Biol.* **61**, 1061–1067 (2012).
682 69. D. M. de Vienne, T. Giraud, O. C. Martin, A congruence index for testing topological
683 similarity between trees. *Bioinformatics*. **23**, 3119–3124 (2007).
684 70. Z. Yang, PAML 4: Phylogenetic Analysis by Maximum Likelihood. *Mol. Biol. Evol.*
685 **24**, 1586–1591 (2007).
686 71. D. T. Ksepka, J. F. Parham, J. F. Allman, M. J. Benton, M. T. Carrano, K. A.
687 Cranston, P. C. J. Donoghue, J. J. Head, E. J. Hermsen, R. B. Irmis, W. G. Joyce, M.
688 Kohli, K. S. Lamm, D. Leehr, J. S. L. Patané, P. D. Polly, M. J. Phillips, N. A. Smith,
689 N. D. Smith, M. van Tuinen, J. L. Ware, R. C. M. Warnock, The fossil calibration
690 database, a new resource for divergence dating. *Syst. Biol.* **64**, 853–859 (2015).
691 72. M. J. Benton, Donoghue, P. C.J., R. J. Asher, M. Friedman, T. J. Near, J. Vinther,
692 Constraints on the timescale of animal evolutionary history. *Palaeontol. Electron.*

**18.1.1FC**, 1–105 (2015).

73. E. Paradis, K. Schliep, ape 5.0: An environment for modern phylogenetics and evolutionary analyses in R. *Bioinformatics*. **35**, 526–528 (2019).

74. Z. Zhang, L. E. Holmer, F. Chen, G. A. Brock, Ontogeny and evolutionary significance of a new acrotretide brachiopod genus from Cambrian Series 2 of South China. *J. Syst. Palaeontol.* **18**, 1569–1588 (2020).

75. A. V. Vinogradov, New fossil freshwater bryozoans from the Asiatic part of Russia and Kazakhstan. *Paleontol. J.* **30**, 284–292 (1996).

76. K. M. Cohen, S. C. Finney, P. L. Gibbard, J.-. X. Fan, The ICS International Chrongostratigraphic Chart. *Episodes*. **36**, 199–204 (2013).

77. R. A. Pohowsky, The boring ctenostomate Bryozoa: taxonomy and paleobiology based on cavities in calcareous substrata. *Bull. Am. Paleontol.* **73**, 1–192 (1978).

78. J. A. Todd, H. Hagdorn, First record of Muschelkalk Bryozoa: the earliest ctenostome body fossils. *Sonderbände der Gesellschaft für Naturkd. Württemb.* **2**, 285–286 (1993).

79. P. D. Taylor, in *Proceedings of the Seventeenth International Bryozoology Conference.*, R. Schmidt, C. M. Reid, D. P. Gordon, G. Walker-Smith, I. P. Percival, Eds. (2019), pp. 147–154.

80. J. E. Winston, A. H. Cheetham, in *Living Fossils*, N. Eldredge, S. M. Stanley, Eds. (Springer New York, New York, NY, 1984), pp. 257–265.

81. M. N. Puttick, MCMCtreeR: functions to prepare MCMCtree analyses and visualize posterior ages on trees. *Bioinformatics*. **35**, 5321–5322 (2019).

82. M. dos Reis, J. Inoue, M. Hasegawa, R. J. Asher, P. C. J. Donoghue, Z. H. Yang, Phylogenomic datasets provide both precision and accuracy in estimating the timescale of placental mammal phylogeny. *Proc. R. Soc. B-Biological Sci.* **279**, 3491–3500 (2012).

718 83. A. Waeschenbach, P. D. Taylor, D. T. J. Littlewood, A molecular phylogeny of
719 bryozoans. *Mol. Phylogenet. Evol.* **62**, 718–735 (2012).
720 84. S. O. Martha, L. M. Vieira, J. Souto-Derungs, A. V. Grischenko, D. P. Gordon, A. N.
721 Ostrovsky, in *Phylum Bryozoa*, T. Schwaha, Ed. (2021), pp. 317–433.
722 85. D. P. Gordon, Apprehending novel biodiversity redux – thirteen new genera and three
723 new families of Zealandian Bryozoa, with the first living species of the
724 Eocene–Miocene genus *Vincularia* Vincullariidae. *J. Mar. Biol. Assoc. United*
725 *Kingdom*. **101**, 371–398 (2021).
726 86. W. D. Lang, The Cretaceous Bryozoa (Polyzoa). Volume 3. The Cribrimorphs - Part 1.
727 *Cat. Foss. Bryozoa Dep. Geol. Br. Museum Nat. Hist.* (1921).
728 87. D. Gordon, The marine fauna of New Zealand: Bryozoa: Gymnolaemata
729 (Cheilostomata Ascophorina) from the western South Island continental shelf and
730 slope. *Mem. New Zeal. Oceanogr. Inst.* **97**, 1–158 (1989).
731 88. D. P. Gordon, in *11th International Bryozoology Association Conference.* , A. Herrera
732 Cubilla, J. B. C. Jackson, Eds. (Smithsonian Tropical Research Institute, Balboa,
733 Republic of Panama, 2000), pp. 17–37.
734 89. P. E. Bock, P. L. Cook, in *Biology and Paleobiology of Bryozoans.*, P. J. Hayward, J.
735 S. Ryland, P. D. Taylor, Eds. (Olsen, & Olsen, Fredensborg, 1994), pp. 33–36.
736 90. S. F. Harmer, On the morphology of the Cheilostomata. *Q. J. Microsc. Sci.* **46** (1902).
737 91. J. López-Gappa, L. M. Pérez, A. C. S. Almeida, D. Iturra, D. P. Gordon, L. M. Vieira,
738 Three new cribrimorph bryozoans (order Cheilostomatida) from the early Miocene of
739 Argentina, with a discussion on spinocystal shield morphologies. *J. Paleontol.* **95**,
740 568–582 (2021).
741 92. A. N. Ostrovsky, P. D. Taylor, Brood chambers constructed from spines in fossil and
742 Recent cheilostome bryozoans. *Zool. J. Linn. Soc.* **144**, 317 – 361 (2005).

743 93. G. M. R. Levinsen, *Morphological and systematic studies on the cheilostomatous*
744 *Bryozoa* (Nationale Forfatterers Forlag, Copenhagen, 1909).
745 94. D. A. Brown, On the polyzoan genus *Crepidacantha* Levinsen. *Bull. Br. Museum*
746 *(Natural Hist. Zool.* **2**, 243–263 (1954).
747 95. K. J. Tilbrook, Cheilostomatous Bryozoa from the Solomon Islands. : 1-386. *St.*
748 *Barbar. Museum Nat. Hist. Monogr. 4 (Studies Biodivers. Number 3)* (2006).
749 96. D. P. Gordon, G. Braga, Living and fossil species of the catenicellid subfamilies
750 Ditaxiporinae Stach and Vasignyellinae nov. *Mémoires du Muséum Natl. d'Histoire*
751 *Nat.* **161**, 55–85 (1994).
752 97. J. P. Caceres-Chamizo, J. Sanner, K. J. Tilbrook, A. N. Ostrovksy, Revision of the
753 Recent species of *Exechonella* Canu & Bassler in Duvergier, 1924 and Actisecos Canu
754 & Bassler, 1927 (Bryozoa, Cheilostomata): systematics, biogeography and
755 evolutionary trends in skeletal morphology. *Zootaxa*. **4305**, 1–79 (2017).
756 98. D. P. Gordon, J. Sanner, in *Bryozoan Studies 2019*, P. N. Wyse Jackson, K. Zágoršek,
757 Eds. (Czech Geological Survey, Prague, 2020), pp. 43–58.
758 99. P. D. Taylor, B. Berning, M. A. Wilson, Reinterpretation of the Cambrian 'bryozoan'
759 *Pywackia* as an octocoral. *J. Paleontol.* **87**, 984–990 (2013).
760 100. J. Ma, P. D. Taylor, F. Xia, R. Zhan, The oldest known bryozoan: *Prophyllodictya*
761 (Cryptostomata) from the lower Tremadocian (Lower Ordovician) of Liujiachang,
762 south-western Hubei, central China. *Palaeontology*. **58**, 925–934 (2015).
763 101. E. Landing, J. B. Antcliffe, M. D. Brasier, A. B. English, Distinguishing Earth's oldest
764 known bryozoan (*Pywackia*, late Cambrian) from pennatulacean octocorals
765 (Mesozoic—Recent). *J. Paleontol.* **89**, 292–317 (2015).
766 102. S. J. Hageman, A. Ernst, The last phylum: occupation of Bryozoa morpho-ecospace
767 (colony growth habits) during the early phase of the Great Ordovician

Biodiversification Event. *Palaeogeogr. Palaeoclimatol. Palaeoecol.* **534**, 109270 (2019).

103. G. Hillmer, A 300-million-year gap in the bryozoan fossil record. *Naturwissenschaften, 78, 123–125.* **78**, 123–125 (1991).

104. A. Ernst, in *Handbook of Zoology: Phylum Bryozoa.*, T. Schwaha, Ed. (De Gruyter, Berlin, 2021), p. 11–55.

**Acknowledgements**

This project is funded by the European Research Council (ERC) under the European Union's Horizon 2020 research and innovation programme (grant agreement No 724324 to L.H. Liow). Extra funding for specific sampling expeditions were provided by the National Science Centre of Poland (grant PANIC/2016/23/B/ST10/01936 to P. Kuklinski), the Assemble Plus (Horizon 2020), the Leverhulme Trust (Research Project Award RPG-2016-429 to A. Waeschenbach), the Russian Science Foundation (grant 18-14-00086 to A. Ostrovsky) and the DISTANTCOM project (CTM2013-42667/ANT to C. Avila). B. Figuerola was supported by Beatriu de Pinós (2019-BP-00183), funded by the AGAUR (Government of Catalonia) and by the Horizon 2020 programme under the Marie Skłodowska-Curie grant (No 801370). The CAML-CEAMARC cruise of RV Aurora Australis (IPY project n°53) were supported by the Australian Antarctic Division, the Japanese Science Foundation, the French polar institute IPEV and the Muséum national d'Histoire naturelle), led by voyage leader, Riddle M.

We thank C. Seid (Scripps Institution of Oceanography), A. M. Bemis (University of Florida), S. Mills (NIWA), K. Moore (Tasmanian Museum and Art Gallery), US Coast Guard and California Dept of Fish and Wildlife and all collectors named in the attached SEM cards,

but especially M. Capa, M. Dick, M. Zabala, C. Avila and R. Tan. The staff at Heron Island Research Station (University of Queensland) and at the Research and Educational Station "Belomorskaya" (Saint Petersburg State University) supported us for fieldwork. Paul D. Taylor and J. Winston discussed earlier versions of this phylogeny with us. We thank A.-H. Rønning, B. L. G. Thorbek and the Norwegian Sequencing Centre and the High-Performance Computing Cluster at the University of Oslo for their assistance. We thank J. Beaulieu for help on the HiSSE package. See SM for permits.

**Author contributions**

RJSO performed the preparation for sequencing, the bioinformatics and phylogenetic analyses, EDM and MHR did the vouchering work, EDM provided the calibration points, EDM and DPG drafted the interpretations, RW contributed to the fossil calibration, EDM, DPG, LV, BB, BF, PK, ONK, NNS, ANO, JGH, JS, RLC, KLV, LC identified the specimens, all authors contributed to the collecting of samples. LHL obtained the funding, coordinated the project, performed analyses downstream of phylogenetic analyses with RJSO and RW, and co-wrote the first draft of the ms with RJSO, EDM and DPG, that all coauthors revised.

The authors declare that they have no competing interests. All data needed to evaluate the conclusions in the paper are present in the main text, the Supplementary Materials (SM) and on Dryad.

**Main text figures and legends**

**Fig. 1. Overview of the major bryozoan clades.** This figure shows non-bryozoan, non-cheilostome bryozoan outgroups (white "fans") and the major cheilostome clades (grey "fans") radiating from our inferred phylogenetic backbone. The colored letters associated with the extant cheilostome clades correspond to those in Figs. S1 and S2. Each "fan" is represented by a genus in that clade, whose full species designation is given here. *Pectinatella magnifica* (class Phylactolaemata) Vuoksa River, Russia (photo by V. Starunov); *Telopora lobata* (class Stenolaemata, order Cyclostomata), Northland, New Zealand (photo by A.M. Smith); *Flustrellidra hispida* (class Gymnolaemata, order Ctenostomata) Damgan, Brittany, France (photo by H. De Blauwe). Cheilostome (order Cheilostomata) clades are illustrated by scanning electron micrographs (see Table S1 for location information for those with BLEED numbers, where BLEED is short for Bryozoa Lab for Ecology, Evolution and Development, based at the Natural History Museum, University of Oslo, Norway: *Steginoporella perplexa* (Steginoporellidae; BLEED1651); *Conopeum seurati* (Electridae) Whangarei, New Zealand (photo by D.P. Gordon); *Tegella cassidata* (Calloporidae; BLEED1245); *Margaretta cereoides* (Margarettidae; BLEED1852); *Nellia tenella* (Quadricellaridae; BLEED1433); *Microporella orientalis* (Microporellidae; BLEED959); *Parasmittina galerita* (Smittinidae; BLEED 1498). In this study, A through G are inferred using 75 (A), 2 (B), 318 (C), 38 (D), 6 (E), 150 (F), 235 (G) sequences (corresponding to taxon-tags presented in Fig. S1 and S2) in which more than half are newly sequenced herein. The seven highly supported (Bootstrap BS > 90%, Fig. S2) ancestral nodes that gave rise to the extant cheilostome clades (A-G) are shown will filled circles (color corresponds with the extant daughter clade). The exception being the ancestral node that gave rise to clade B (BS 64%). Each extant clade is highly supported (Bootstrap BS > 90%, Fig. S2).

**Fig. 2. Fossil-calibrated bryozoan tree.** The topology is based on our trimmed tree (Fig. S2). Posterior distributions, based on the "STL" age priors and an independent molecular clock (see Fig. S3 for joint time priors), are shown in grey and salmon-pink, where the latter are nodes used for calibration (roman numerals correspond to those in Table S4). This figure spans two pages.

**Fig. 3. Lower section of cheilostome tree with parental care states.** The topology shows the lower part of the cheilostome tree where brooders with non-feeding larvae are marked in dark blue and non-brooders with planktotrophic (feeding) larvae are marked in light blue. For the probability of transition of every node, including those not shown here, see Fig. S5. Numbers show the transitions to a brooding state that are inferred, where transition 1 (as early as the Carboniferous Figs. 2, S5) led to *Scruparia* (with a skeletal ovicell-like brood chamber), transition 3 (as early as the Jurassic) led to *Eucratea* (with external membranous brooding sacs), transition 4 (as early as the Triassic) to the clade including *Steginoporella* (some with internal brooding sacs and others with skeletal brood chambers), and transition 5 (as early as the Triassic) to 'neocheilostomes' (cheilostomes with brooding structures called ovicells or brooding sacs). See SM for a discussion of transition 2.

857 **Table 1. Comparison of trait-(in)dependent models of diversification.** Models of
858 speciation and extinction rates of non-brooding and brooding cheilostomes are compared
859 using Akaike criteria. The bolded model (cid2, a character independent model that is the
860 "null" version of a binary state (BiSSE) model) has the AIC highest model weight in this set
861 of models, followed closely by a more complex character-independent model (cid4). See
862 Table S7 for results based on other topologies.
863

| Model | Log Likelihood | AIC model weight |
|---|---|---|
| Null | -254.163 | 5.20E-06 |
| BiSSE | -248.735 | 4.22E-04 |
| **cid2 (BiSSE null)** | -240.472 | **0.581** |
| cid4 (HiSSE null) | -238.748 | 0.402 |
| HiSSE | -239.791 | 0.017 |

864
865

**Supplementary Text for Methods**

1. Choice of outgroups

We selected both bryozoan and non-bryozoan (metazoan) outgroups for our phylogenetic inferences and fossil calibrations, given their availability in NCBI and supplemented these with sequences from non-cheilostome bryozoan outgroups newly sequenced within this study. There are three extant, non-cheilostome clades of bryozoans, namely phylactolaemates (represented by *Cristatella* and *Pectinatella* from NCBI in our trees), cyclostomes (represented by *Tubulipora* from NCBI and *Crisia, Spinihornera, Heteropora,* and two *Telopora* species we newly sequenced), and ctenostomes (represented by *Flustrellidra* and *Alcyonidium* from NCBI and another *Flustrellidra* specimen we newly sequenced). In addition, diverse short-branching lophotrochozoans (given our set of taxa represented) which provided nodes that were amenable to fossil calibration were also chosen. A notable absence among the lophotrochozoan outgroup is Mollusca as they were polyphyletic and had long branches in our preliminary analyses, given our choice of genes extracted for the bryozoan ingroup. In addition to those stated above, a common criterion for the selected sequences from NCBI was the availability of a mitochondrial genome.

2. Choice of fossil calibration points

We selected 18 primary fossil calibration points for our tree. Four of these are non-bryozoan calibrations, where we base our input on the Fossil Calibration Database (*71*) with the exception of Brachiopoda, whose oldest described fossil is placed in Cambrian Stage 2 c. 529 to 521 Mya (*74*). In all cases where an age range is given for a fossil, we conservatively use the upper bound as a minimum age. We discuss our bryozoan calibrations briefly below and tabulate all calibration points in Table S4, and illustrate the joint prior age distributions given only the tree topology in Fig. S3.

We do not input any calibration for phylactolaemates, whose fossil record is based solely on statoblasts and where most examples are from the Holocene and Pleistocene. Although there are records of statoblasts from as early as the Permian (*75*) these ages are severe underestimates for the phylactolaemate lineage, which is sister to all other living bryozoan groups, namely ctenostomes, cyclostomes and cheilostomes, all which have older fossil records (see paragraphs below). We also note that we do not consider the Cambrian fossil *Pywackia baileyi* a bryozoan (see section 6 below). However, as already mentioned in the main text, we note that there are now highly reliable observations of Cambrian bryozoan fossils, newly named *Protomelission* (*9*). In each case detailed below in this section, we select the oldest known fossils of the groups for which we could verify the morphology of the named species with an available Scanning Electron Micrograph or at least a high-quality photograph, and where the stratigraphy has been confirmed. All fossil ages, if not specified numerically in the reference describing the species, are based on our understanding of the described stratigraphy using the updated online version (v 2020/01) of the International Chronostratigraphic Chart (*76*).

The oldest known fossil cyclostome is *Wolinella baltica* Dzik, 1981. This fossil has been assigned to the Volkhov Stage of the Early Ordovician (corresponding to the Arenigian 478.6–471.8 Mya, where Mya = million years ago).

The oldest known fossil ctenostome is *Ropalonaria venosa* Ulrich, 1879 an endolithic ctenostome from the Upper Ordovician (Cincinnatian Series) of the Waynesville Formation (Katian) (*77*). We give this fossil an estimated age of 453–445.2 Mya (from the bottom to the top of the Katian). Note that the first body fossil (bioimmured) of ctenostomes is from the Ladinian in the Middle Triassic (*78*).

914 The oldest known fossil of Cheilostomata is *Pyriporopsis pohowskyi* Taylor, 1994
915 from the Oxfordian-Kimmeridgian. We hence put the age of this fossil at 163.5–152.1 Mya
916 (from the base of Oxfordian to the top of Kimmeridgian).
917
918 Three oldest known *Steginoporella* species have their earliest appearance in the
919 Lutetian (47.8–41.2 Mya) namely *S. asymetrica* (Canu, 1907), *S. firma* (Canu, 1907) and *S.*
920 *immanis* (Canu & Bassler, 1929). Note that the taxonomic status for *S. rhomboidalis* (Hennig,
921 1892) found in the Campanian of Sweden is uncertain and we do not use it here. Likewise,
922 the oldest known *Labioporella*, *Calpensia* and *Thalamoporella*, respectively *L. dartevillei*
923 Cheetham, 1966, *C. profunda* Canu, 1919, and *T. minuta* Guha & Gopikrishna, 2004, *T.*
924 *domifera* Guha & Gopikrishna, 2004, *T. dorothea* Guha & Gopikrishna, 2004 are all from the
925 Lutetian. We hence use the top of the Lutetian as a minimum for this clade.
926 Several species of *Lunularia* are known from the Cretaceous (Campanian 83.6–72.1
927 Mya), namely, *L. declivis* and *L. marssoni* (Brydone, 1911) from England, and *L. excavata*
928 (Hennig, 1892) from Sweden.
929 *Electra everretti* Taylor & McKinney, 2006 is the oldest confirmed *Electra* from the
930 Peedee Formation of North Carolina, USA, which is assigned to the Maastrichtian (72.1–66
931 Mya).
932 The earliest known species of Monoporelloidea is *Monoporella* sp. (*79*) from the
933 Campanian–Maastrichtian (83.62–66 Mya, from the bottom of the Campanian to the top of
934 the Maastrichtian) of Need's Camp near East London in Cape Province, South Africa.
935 The earliest known *Cellaria* is *C. inaequalis* d'Orbigny, 1851 from the Late
936 Cretaceous (Campanian–Maastrichtian, 83.6–66 Mya) of France, Charente-Maritime, where
937 we confirmed its identity with the publicly available syntype image from the
938 https://science.mnhn.fr website.

939 The earliest known *Adeonellopsis* and Adeonidae is *Adeonellopsis incompta* Gordon
940 & Taylor, 2015 from early Waipawan (Eocene, Ypresian 56.5–52 Mya).
941 The earliest known *Nellia* is from the Maastrichtian of Jamaica (72.1–66 Mya) as
942 noted in (*80*).
943 The earliest known *Microporella* is *M. waghotensis* Guha & Gopikrishna, 2007 from
944 the Aquitanian (23.03–20.44 Mya) Gujarat, India. Note that *M. fallax* Canu, 1904 from the
945 San Julian Formation of Bajo di San Julian, Argentina is not published with adequate
946 imaging or drawings and has an uncertain identity as such. Its purported Paleogene age is also
947 uncertain and we hence do not use it as a calibration even though it could be older (but also
948 younger) than *M. waghotensis*.
949 The earliest known *Fenestrulina* is *F. harmelini* David, Mongereau, & Pouyet, 1972
950 from the Burdigalian (20.44–15.97 Mya) of France.
951 The earliest confirmed record of Celleporidae is *Osthimosia aurora* Gordon & Taylor,
952 2015 from the Chatham Islands with an estimated age of early Waipawan (56.5–52 Mya).
953 The earliest confirmed record of Phidoloporidae is *Reteporella mediocris* Gordon &
954 Taylor, 2015 also from the Chatham Islands with an estimated age of early Waipawan (56.5–
955 52 Mya).
956 The earliest known *Parasmittina* are *P. harudiensis* Guha & Gopikrishna, 2005 and *P.*
957 *gujaratica* Guha & Gopikrishna 2005, both from the Lutetian (47.8–41.2 Mya) of India
958 Gujarat. We include *Pleurocodonellina* as a descendent of the *Parasmittina* lineage due to
959 their very close morphological affinity.
960
961 3. MCMCTREE settings
962 Distribution parameters for node calibrations implemented in MCMCTREE (*70*) were
963 obtained using the R package MCMCTreeR (*81*). We used the GTR G4 model for the

964 nucleotide dataset (partition) and MTZoa for the amino acid dataset. The alpha parameter for
965 gamma distributed rate variation across sites was estimated using RAxML (*66*) for each
966 partition. The overall substitution rate and variance parameter are specified using a gamma-
967 Dirichlet prior. For the prior on the mean rate of each locus we used a gamma
968 distribution G(2, 20), which has a mean of 0.1 changes per site per 100 million years, while
969 the relative variation across loci is specified using a symmetric Dirichlet distribution with
970 alpha = 1. For the prior on the variance parameter we used a gamma distribution G(1, 10) and
971 a symmetric Dirichlet distribution with alpha = 1. The branching process prior, the
972 parameters of the birth-death process (birth, death and species sampling) were set to 1, 1 and
973 0.1, as we have sampled about 10% of all described species. This combination of parameters
974 produces a broad prior on the node ages of uncalibrated nodes, chosen to represent a large
975 degree of uncertainty. MCMC runs for each set of calibrations were first carried out without
976 sequence data to estimate the effective joint time priors and to check for consistency with the
977 specified fossil calibrations. MCMC chains were twice run for 1.7 million generations with
978 10% burn-in for each combination and convergence ensured. Mixing for each chain was
979 checked by inspecting the effective sample size (ESS) and the traces of each node. As the
980 exact calculation of the likelihood function during Markov chain Monte Carlo (MCMC)
981 iteration is computationally heavy, we employed an approximate method (*82*). Joint time
982 priors and posterior distributions of node ages are figured using the R package MCMCTreeR
983 (*81*).
984
985 4. Taxonomic name updates after the selection of a further pruned tree for calibration.
986 The dataset described in section *2.7.* in the main text *"Fossil-calibration and Bayesian*
987 *divergence time estimation"* was selected before the following updates of names listed below:
988

Two of the sequenced specimens we previously labelled as “unknown” have been united with our SEM card vouchers and they are hence:

UNKNOWN_SEQ_BLEED1948 = *Marcusadorea* sp. BLEED 1948

UNKNOWN_SEQ_BLEED1866 = *Thrypticocirrus phylactelloides* BLEED1866

Two sequences that were thought to be contaminants of the macroscopic, vouchered specimens (*Hippoporina indica*) are reinstated as we confirmed these sequences with very high identity (BLEED 839 and BLEED 1248) from two very different localities, California and Singapore. *H. indica* is an invasive species that is actually quite well known https://invasions.si.edu/nemesis/species_summary/-453 and appears to be nested within the very well sampled *Parasmittina* clade. They are:

*Parasmittina*_sp_SEQ_BLEED839 = *Hippoporina indica* BLEED839

*Parasmittina*_sp_SEQ_BLEED1248 =*Hippoporina indica* BLEED1248

None of these appear in the calibrated trees (Fig. 2 and Fig. S3) but their phylogenetic positions can be found in Figs. S1 and S2 (as the updated names, and the same BLEED numbers).

**Supplementary Text for Results and Discussion**

1. Extended discussion of the RAxML tree

The inferred phylogeny (Fig. 1, Fig. S1 and S2) we present is large and suggests both controversial and less controversial hypotheses. The cheilostome "fan blades" in Fig. 1 each include a total followed by samples new to this study A 68:51, B 2:0, C 267:126, D 30:11, E 5:5, F 122:63 and G 197:130 for Fig. S2. Likewise, for the full tree (Fig. S1): A 75:57, B 2:0, C 318:169, D 38:19, E 6:6, F 150:90 and G 235:166. We present and discuss a selection of key observations that may be of interest to specialists here. We also note that the specialist may notice further apparent phylogenetic affinities presented in the inferred topologies that we do not discuss. All topological inferences should be interpreted while considering the bootstrap values associated with those nodes and the taxon sampling around those nodes (as exemplified below).

The general structure of the cheilostome phylogeny presented here corresponds to that inferred in an earlier publication (*20*), where $I_{cong}$ index = 8.41; probability that they are topologically unrelated = 2.15e-101, based on the index suggested by (*69*). As mentioned in the main text, our phylogeny has a well-supported backbone (Fig. 1) and a relatively high mean bootstrap (BS) support of 88.94% per node (calculated based on Fig. S2 with 721 taxa). The latter is comparable to a mean BS support of an earlier but less broadly taxonomically sampled tree with 165 species (*20*) at 89.95% per node.

Some nodes that were less supported before [e.g. (*Rhynchozoon* + *Stephanollona*), (*Phidolopora*, *Hippellozoon* and *Iodictyum*) BS 62% in (*20*)] have greatly improved support, with newly sequenced genera added to each of these clades (e.g. *Dentiporella, Plesiocleidochasma,* Fig. S2). Another such example is [(*Bugula*+*Bicellariella*), (*Beania*)] which had only 51% BS support, but now has 100% BS support, with many of the taxa that were previously not sequenced and included filling the taxon "space" between the more

distantly related taxa. Support for some other nodes "worsened" compared with those in (*20*) [e.g. (*Caleschara),* (*Cellaria*+*Steginocellaria*)] but there is more taxonomic resolution with newly added taxa (e.g. *Melicerita, Swanomia*).

Of the seven highlighted extant clades, that emerged from the corresponding ancestral diversions from the cheilostome backbone (Figs. 1, S1 and S2), *Conopeum* deserves a special mention as it is relatively poorly supported. An earlier molecular study inferred *Conopeum* as the earliest diverging cheilostome based on a handful of genes (*83*), giving support to the general view of its simple zooidal morphology, planktotrophic larvae, and lack of embryonic incubation (brooding). Its molecular phylogenetic placement in our inference, based on 17 genes, is different from that inferred in (*83*), such that it is plausible *Scruparia* (with lecithotrophic larvae and ovicell-like brood chamber, both thought to be more derived traits) could have evolved from the earliest diverging branch of cheilostomes instead (*84*). This "*Conopeum*/*Scruparia* challenge" also highlights the cryptic phylogenetic diversity among genera currently placed in the family Electridae, members of which have relatively few phenotypic characters (*85*). However, we do note that our ancestral state reconstruction infers that a non-brooding/planktotrophic state is basal, so even if the lineage of *Scruparia* is sister to all other extant cheilostomes, the lineage leading up to the extant representative we sequenced would have transitioned from non-brooding/planktotrophic to brooding/non-feeding some time before the Recent. Note also that because an alternative topology with respect to *Conopeum* may affect our inference in the analyses of brooding and speciation, we ran analyses without *Conopeum* as sister to all extant cheilostomes as part of our sensitivity analysis (see results in Table S7 and also later paragraph on *Lunularia*).

While most genera are inferred to be monophyletic or at least paraphyletic, a few (especially those that have not been taxonomically revised for a long time) are not, e.g. *Smittina* and *Porella.* As we wrote in the main text and in an earlier paper (*20*), higher

cheilostome taxa such as families and superfamilies are currently often poorly circumscribed and defined. For example, Smittinidae, including *Smittina*, *Parasmittina*, *Smittoidea* and the newly sequenced *Thrypticocirrus*, *Pemmatoporella*, *Raymondcia* are scattered throughout clade G. Likewise Bugulidae, including *Beania* and the newly sequenced *Bugulopsis*, *Dendrobeania*, *Crisularia*, *Virididentula*, are scattered throughout clade C (see Figs. S1, S2). In some cases, phenotypic hypotheses suggested by our molecular phylogeny could help to resolve debates in the systematic literature.

For instance, it has long been suspected that the family Cribrilinidae s.l. (= "cribrimorphs") is polyphyletic (*86*), where ancestors with articulated periopesial spines evolved non-articulated spines (costae) more than once (*87*, *88*). This is supported not only by the association of *Cribrilina* and *Juxtacribrilina* with non-spinocystal taxa (*Klugeflustra* and *Valdemunitella*) but their clear separation from *Puellina* and *Cribrilaria*, which have more-complex pinnate costae. *Euthyroides*, also in the same clade in our tree, contains either species with gymnocystal frontal shields either species having a few or vestigial costae. While the inference of *Retiflustra* as belonging to the same clade is somewhat more surprising, we do not have reason to believe it is problematic as plausible evolutionary-developmental scenarios can explain its phylogenetic position: we speculate that developmental suppression of spines could result in non-costate morphology (such as in *Retiflustra*). Such suppression has been observed in *Corbulipora tubulifera* (currently placed in Cribrilinidae) which manifests costate and non-costate zooids in the same colony at different stages of development (*89*). See (*86*, *90*) for early discussions on the polyphyly of cribrimorph taxa and (*91*) for a modern one.

On the basis of detailed morphological analyses of brood chambers in the anascan families Thalamoporellidae and Steginoporellidae (*19*), Ostrovsky concluded that the phylogenetic and development origins of these structures had to have been independent of

1081 that in other anascans. Ostrovsky (*19*) consequently introduced a new suborder,
1082 Thalamoporellina, to accommodate them. Our results, where *Steginoporella*
1083 (Steginoporellidae), *Labioporella* (Steginoporellidae), *Thalamoporella* (Thalamoporellidae),
1084 *Dibunostoma* (Thalamoporellidae) form a well-supported clade, support Ostrovsky's
1085 conclusions. We note that *Calpensia,* which is well-nested within the clade containing
1086 Steginoporellidae and Thalamoporellidae, lacks an external ovicell-like chamber and is
1087 thought to have an internal brood sac, like in *Steginoporella*. In another example, the ovicells
1088 of *Macropora* (Macroporidae) and *Monoporella* (Monoporellidae) were found to be
1089 constructed from basally articulated spines or costae (*92*), and the superfamily
1090 Monoporelloidea was hence erected to accommodate both families (*19*), a hypothesis based
1091 on morphology that is now 100% supported by the available molecular data (Figs. S1, S2).
1092 Other morphological hypotheses are perhaps somewhat more debated than
1093 Thalamoporellina and Monoporelloidea in the above-paragraph, but are also potentially
1094 resolvable based on our inferred topology. It has been argued, for instance, that a fully
1095 cryptocystal-anascan shelf and orifice-like opesia are evolutionarily derived from the
1096 expansion of a narrow periopesial cryptocyst (*84*, *93*). This evolutionary hypothesis is
1097 supported by the close association of *Parellisina* and *Copidozoum* (calloporids with a narrow-
1098 to-moderate cryptocyst) with *Opaeophora* (extensive cryptocystal shelf), demonstrating that
1099 the latter cannot be included in ‘core’ Microporidae (i.e. based on the type genus *Micropora,*
1100 including also *Promicroa and Puncturiella*). Both Calloporidae and Microporidae are in dire
1101 need of study and taxonomic revision.
1102 A pedunculate avicularium that can resemble a bird's head appears to have arisen
1103 independently three times—in core Buguloidea consisting of Bugulidae (*Bugula*,
1104 *Bicellariella*, *Bugulina*, *Camptoplites*, *Caulibugula*, *Cornucopina*, *Crisularia*, *Dendrobeania*,
1105 *Halophila*, *Himantozoum*, *Virididentula*) and Beaniidae (*Beania*), Epistomiidae (*Synnotum*)

and Euoplozoidae (*Euoplozoum*). The latter two families (currently assigned to Buguloidea (*17*)) can be excluded from Buguloidea based on our inferred phylogeny, hence the birds-head avicularium in Buguloidea as newly circumscribed here, can be considered homologous.

The affinities of *Crepidacantha* have long been regarded as problematic (*94*). Based on the superficial similarity of the pseudoporous ovicell in some *Crepidacantha* species to that in Mamilloporidae (consisting of *Anoteropora* and *Mamillopora* which we did not have samples of for sequencing), D.P. Gordon included the Crepidacanthidae in the superfamily Mamilloporoidea in an unpublished classification of Cheilostomata for the Treatise on Invertebrate Paleontology. This treatment is currently accepted (*95*), and is used on the Bryozoa Home Page (*17*). In our molecular phylogenetic inference, *Crepidacantha* is well nested in superfamily Adeonoidea where characters shared with *Crepidacantha* include numerous basal pore-chambers. It remains to be seen if *Anoteropora* and *Mamillopora* might be closely allied with Adeonoidea.

Some relationships, such as the likely derivation of foraminate-shielded Arachnopusiidae (*Arachnopusia*) from anascan Foveolariidae (*Foveolaria*) previously noted (*20*), continue to be supported with greater taxon sampling in the current study, although in this particular case, no new specimens attributed to these families are sequenced. In the case of *Celleporaria*, however, we added taxonomic sampling both within the genus and around it (Fig. S2) and corroborate our previous inference that *Celleporaria* should be reinstated in Celleporidae, despite its umbonuloid frontal shield (*20*).

Given both the incomplete taxon sampling and a limited set of genes within our study, we did not expect all the relationships we have inferred to be highly-supported, and/or morphologically “logical”, given what we know today. For example, the association of Catenicellidae (*Orthoscuticella*, *Scuticella*, *Paracribricellina*, *Costaticella*, *Talivittaticella, Pterocella*, *Cornuticella* and *Terminocella* in our trees) with Myriaporidae

(*Myriapora*), Margarettidae (*Margaretta*), Porinidae (*Porina*), Gigantoporidae (*Cosciniopsis* and *Gigantopora*) and Exechonellidae (*Exechonella*) is morphologically challenging. *Margaretta*, *Myriapora*, *Porina* and Gigantoporidae all have pseudoporous lepralioid frontal shields and are conceivably evolutionarily closely related. But *Exechonella* is umbonuloid while catenicellids have a cribrimorph frontal shield (*96*). The tantalizing plausibility that the frontal shield in *Exechonella* could have evolved from flattened costae (*97*) suggests that its current phylogenetic placement could be congruent with morphology. Yet, it is clear from the support values of these relationships (mostly < 40% BS, some with single digit support, see Figs. S1, S2) that this current picture is likely to be modified with greater gene and taxon sampling, and not least, increased efforts in studying the development and morphology of these taxa.

Perhaps more puzzling is the very highly-supported relationship between the gymnocystal-shielded Eurystomellidae (*Eurystomella*, *Integripelta*) and the cryptocystal-shielded Euthyrisellidae (*Euthyrisella*). Euthyrisellidae may have conceivably had a microporoidean-type ancestor with a perforated cryptocyst (*98*) as also suggested by our trees (Figs. S1, S2). But why the Eurystomellidae is part of the highly-supported clade requires pondering. As these relationships are exemplified by multiple species/specimens of their genera, we have strongly reduced the plausibility of sample contamination as an explanation. We also expected *Euoplozoum* to be allied with the Bugulidae, based on morphology, but given that we only have a single representative of this genus, we cannot completely rule out the possibility that we have not sequenced our target *Euoplozoum.* This can only be alleviated by sequencing other samples of *Euoplozoum.*

We also note here that the inferred phylogenetic position of *Lunularia* is also curious as it is believed to be a cheilostome that diverged later based on its avicularia and internal brooding in a brood sac. However, the sequences present in the sample BLEED1770

contained only one cheilostome species, 15 out of 17 genes were extracted in our pipeline and the BS support of this node is high and has a relatively large distance to the most closely related taxon (*Aetea*). If it had been more similar in its sequences to *Aetea*, we might have assumed that it was an *Aetea* contaminant. Note also that *Aetea* was removed from downstream analyses as it had unstable phylogenetic affinities (see main text). As this single taxon may affect our inference in the analyses of brooding and speciation, we ran analyses without *Aetea* as part of our sensitivity analysis (see results in Table S7).

2. Extended discussion on novel and hidden diversity from target and non-target bryozoans

Bryozoan taxonomy is steadily uncovering new species and the rate of discovery is limited by the number of available experts rather than sampling efforts. In this study, we aimed to sequence described species but serendipitously, we also sequenced many species which are unnamed or even observed and documented for the first time (those labeled n. sp. in Table S1 and our SEM cards, available as SM). The 17 species (c. 4% of colonies newly sequenced that have physical vouchers) new to science (including one likely to require a new genus name, see BLEED952 and BLEED1054 in Fig. S1 and SEM cards) we sequenced are likely an underestimate as we also have taxa for which our morphological vouchers were not pristine enough to either assign a taxonomic name or recognize the specimen as a new taxon (i.e. those labelled only sp. in Table S1). While some of these are likely to be previously described species, others could also be taxa new to science.

As mentioned in the main text, we also present sequences that are not target species but for which we have found enough of the contaminant for imaging (e.g. BLEED420A was our targeted *Iodictyum* cf. *ornithorhyncus* while BLEED420B *Reteporella* aff. *tuberosa* was a contaminant that was later vouchered; BLEED1115B *Xenogma rhomboidale* was the target and 1115A *Fenestrulina* sp. was the vouchered contaminant, likewise for 1818A and B

*Margaretta* and *Lagenicella,* just to give a handful of examples from Fig. S1). Note also that the use of letters following BLEED numbers are an indication of the presence of non-target bryozoans, even if not all target/non-target sequences are necessarily presented here (e.g. they could have been excluded due to extraction of too few genes in our pipeline).

We also uncovered both known and currently unmatched non-target species among our samples that do not have remaining physical vouchers because our pipeline from DNA isolation to genome-skimming extracts high-copy sequences from any cheilostome sequences present in our target sample. For example, given our taxon sampling and observed sequences, we are certain that some non-target sequences (with no physical material that can be vouchered) belongs to a given genus, e.g. *Galeopsis* BLEED1367, *Fenestrulina* BLEED977, *Microporella* BLEED400B, *Valdemunitella* BLEED1617 (Fig. S1). In a few cases, we are confident that the unvouchered sequences belong to a specific species. For example, SEQ_BLEED787 (labelled as "*Microporella_appendiculata_* SEQ_BLEED787") has no genetic distance (given the genes we analyzed) to *Microporella appendiculata* BLEED1858 for which we have a physical voucher, see Fig. S1). The target sample in BLEED787 was a cyclostome (*Crisia*) for which we have both sequences and a physical voucher. BLEED787 and 1858 are from different locations in the Mediterranean, collected on different dates by different people and two samples were processed and sequenced on different dates, so there is little to no chance of contamination.

In other cases, the sequence data do not nest in a clade within our tree, e.g. UNKNOWN_SEQ_BLEED1699 and UNKNOWN_SEQ_BLEED1702 and are hence labeled as "unknowns". We are in general conservative in giving sequences taxon names and urge further investigation of the remaining samples or colony fragments to yield more morphological information in future studies.

Note also that there are some previously sequenced specimens (i.e. they have already been vouchered in association with previous publications) for which we have re-sequenced the same colony or improved on our bioinformatic pipelines (e.g. BLEED387, BLEED800).

3. Extended discussion of the fossil-calibrated tree

Our fossil calibrated tree shows the origins of bryozoans to be in the Cambrian or even the Ediacaran (Fig. 2). The lack of a fossil record of bryozoans in the Cambrian, where all other skeletal metazoan phyla have fossil representation, has always been a curious observation (*99*), although this enigma has very recently been resolved with the description of *Protomelission* (*9*). Previously, the earliest confirmed fossil of a bryozoan is the cryptostome *Prophyllodictya simplex* Ma, Taylor, Xia & Zhan, 2015 from the lower Tremadocian (Lower Ordovician) of China (*100*). The late Cambrian fossil *Pywackia baileyi* Landing, 2001, has been on occasion attributed to a bryozoan. Taylor et al. (*99*) re-interpreted *Pywackia* as a pennatulacean octocoral, but Landing et al. argued against this reinterpretation (*101*). The latest interpretation is based on skeletal microstructure and taphonomy (Hageman 2018 cited in (*102*)) which shows further evidence that *Pywackia* is not a bryozoan.

Our fossil calibrated tree shows the origins of cheilostomes to be Carboniferous or Devonian (Fig. 2). The earliest putative cheilostome, *Schallreuterella syltensis* Hillmer, 1987, was suggested to be Ordovician (*103*). The zooids were paired at intervals along narrow kenozooidal stems making up jointed branches, and each zooid was box-like and apparently operculate. Hiller (*103*) hypothesized that Cheilostomata leading to *Schallreuterella* may have originated from a stenolaematous ancestor resembling *Corynotrypa* (Cyclostomata). Ernst (*104*) interprets *Schallreuterella* as a species of Fenestrata and both he and Taylor (*7*) concur that *Schallreuterella* is a case of evolutionary convergence and not a cheilostome. Based on existing published fossil evidence, there is currently no candidate taxon that would

1230 serve as a putative ancestor to crown-group Cheilostomata. The only fossils are those
1231 pertaining to several orders of Stenolaemata, all of which are inferred to have had a very
1232 different mechanism for lophophore extrusion. The gymnolaemate order Ctenostomata is
1233 known from early Paleozoic borings but there are no body fossils. Notwithstanding,
1234 Ctenostomata remains the most likely ancestor for cheilostomes.
1235
1236 4. Evolution of parental care and speciation rates of brooders: sensitivity analyses
1237 Because there are few non-brooders among cheilostomes and they all seem to be lineages that
1238 have diverged early in cheilostome history, the trait-based speciation and extinction models
1239 we fit (BiSSE, HiSSE and their null versions) will be sensitive to the topology at the base of
1240 the cheilostome tree. There are two taxa (*Conopeum* and *Lunularia*) whose placement are
1241 contentious, as mentioned in the main text and section 4 in this SM (see above). It is
1242 plausible that a contaminant rather than the true *Lunularia* has been sequenced, based on our
1243 understanding of morphological evolution, hence we used a topology where this taxon is
1244 completely removed in our trait-based BiSSE/HiSSE analyses. *Conopeum* has a relative weak
1245 BS support in our tree and has previously be inferred to be sister to all other extant
1246 cheilostomes and hence we used another topology where this taxon branches off first in the
1247 cheilostome tree.
1248 The results of the alternative AIC weights for the five SSE models are shown in Table S7,
1249 where we repeat the results from the main text for easy comparison. The alternative
1250 topologies both show a Hidden State model (HiSSE) as the best model, where the inference is
1251 that a “hidden” or currently unmeasured trait that is associated with (non)-brooding drives
1252 differences in diversification rates among cheilostomes. What this trait might be requires
1253 further exploration that is outside of the scope of this current analysis. We also note that the
1254 number of times non-brooding has transitioned to brooding would have happened one time

1255 less given the removal of *Lunularia* (given the taxon sampling in this study). Note that it has
1256 been hypothesized that a transition to brooding (embryonic incubation and non-feeding
1257 larvae) occurred 7 times in cheilostome history (*19*), but we were not able to successfully
1258 sequence other key taxa (e.g. *Tendra*, *Heterooecium*, *Leiosalpinx, Bellulopora*) that might
1259 have lent support to this hypothesis.
1260
1261 5. Sampling and sample permits
1262 All new samples presented in this paper are collected and sequenced legally and
1263 where applicable conforming to the Nagoya Protocol. The following are a list of permit
1264 numbers where applicable with the initials of the responsible coauthors in parentheses.
1265 Great Barrier Reef specimens collected under the following permits (RC): Seabed
1266 Biodiversity Project — Great Barrier Reef Marine Park Authority Collection Permit
1267 G03/7584.1, G05/14726.1; CReefs Project 2008–2010 — Great Barrier Reef Marine Park
1268 Authority Collection Permit G08/27858.1 (RLC). Western Australian specimens collected
1269 under the following permits: SF010720, (DoF) 2721; SF010627, (DoF) 2677 (RLC).
1270
1271 Heron Island: Great Barrier Reef Marine Park Authority collecting Permit G17/40024.1
1272 (AW). Tasmanian Government Department of Primary Industries, Parks, Water &
1273 Environment - Wild Fisheries Branch Scientific Permit (Fauna) number 17145 (AW).
1274 Singapore National Parks Board permit number: NP/RP19-006 (DWH).
1275 Australian Antarctic Division Chief Scientist Michael Stoddart for AAS Project
1276 2792 *Australia's Census of Antarctic Marine Life project.* PERMIT VARIATION:
1277 AMLR 07-08-2792 VAR1 (PK). DISTANTCOM project (CTM2013- 42667/ANT) funded
1278 by the Spanish government (BF). AREX 2018 RV OCEANIA Permit 18/8560 (PK). South
1279 African permit numbers: RES2017/52, RES2016/09, RES2009/49 (WF). Specimens

attributed to the Smithsonian Institute are collected with permission of the California Department of Fish and Wildlife (Permit no. S-191360002-19136-001) and funded by the United States Coast Guard, Dept. of Homeland Security and the State of California, Dept of Fish and Wildlife's Marine Invasive Species Program (LM). Specimens provided from the NIWA Invertebrate Collection were collected on numerous surveys including: Biodiversity survey of the western Ross Sea and Balleny Islands (TAN0402) undertaken by NIWA and financed by the former New Zealand Ministry of Fisheries (MFish); Oceans Survey 2020 Southern Colville Ridge (TAN1313) voyage, funded by Land Information New Zealand (LINZ) and GNS Science; Fisheries research trawl surveys conducted by NIWA and funded by Fisheries New Zealand (FNZ); Interdisciplinary New Zealand-Australian "MacRidge 2" research voyage (TAN0803), the biological component of which was part of NIWA's research project "Seamounts: their importance to fisheries and marine ecosystems" funded by the New Zealand Foundation for Research, Science and Technology (FRST) and CSIRO's Division of Marine and Atmospheric Research project "Biodiversity Voyages of Discovery" funded by the CSIRO Wealth from Oceans Flagship; Kerry Walton, University of Otago; Seamounts project (TAN0905) undertaken by NIWA and funded by FRST, with complementary funding from MFish; Scientific Observer Program funded by FNZ; Biogenic Habitats on the Continental Shelf project (voyages TAN1105 & TAN1108), funded by New Zealand Ministry for Primary Industry (MPI), FRST, NIWA and LINZ; Ocean Survey 20/20 Bay of Islands Coastal Biodiversity, Sediment and Seabed Habitat Project (TAN0906, KAH0907), funded and owned by LINZ; Ocean Survey 20/20 Mapping the Mineral Resources of the Kermadec Arc Project (TAN1104), funded by LINZ, GNS, NIWA and Woods Hole Oceanographic Institution; Oceans Survey 2020 Reinga (TAN1312) voyage, funded by LINZ and New Zealand Petroleum & Minerals; Impact of resource use on vulnerable deep-sea communities project (TAN1503), funded by the Ministry of Business,

Innovation & Employment (MBIE) with support from MPI; Joint Japan-Tonga Trench leg of the Quelle 2013 Expedition (YK13-10), funded by JAMSTEC and supported by NIWA; Food-web dynamics of New Zealand marine ecosystems supported by the New Zealand government under "Coasts & Oceans" core funding from MBIE (DPG). Samples with museum numbers (see SEM cards), if not accounted for by the listed permits, are associated with museum collection permits.

**Supplementary Figures**

**Fig. S1A. Phylogeny based on the full alignment.** S1A shows the inferred maximum likelihood topology (the letters A through G correspond to the major, and extant cheilostome clades in Fig. 1, with the ancestral backbone node, and corresponding BS support, that gave rise to this clade highlighted with the matching color) of the inferred phylogeny of bryozoans and outgroups**.** This is based on 854 taxa (823 cheilostomes) with 9172 nucleotide and amino acid characters (18 genes) with bootstrap values (shown at nodes) inferred using RAxML. Tips are labelled with Taxon tags corresponding to those in Tables S1 and S2. *This figure is supplied as a separate file.*

**Fig. S1B. Phylogeny based on the full alignment.** S1B shows the inferred maximum likelihood cladogram (the letters A through G correspond to the major cheilostome clades in Fig. 1, with the ancestral backbone node, and corresponding BS support, that gave rise to this clade highlighted with the matching color) of the inferred phylogeny of bryozoans and outgroups**.** This is based on 854 taxa (823 cheilostomes) with 9172 nucleotide and amino acid characters (18 genes) with bootstrap values (shown at nodes) inferred using RAxML. Tips are labelled with Taxon tags corresponding to those in Tables S1 and S2. *This figure is supplied as a separate file.*

**Fig. S2A. Phylogeny based on the trimmed alignment.** S2A shows the inferred maximum likelihood topology (the letters A through G correspond to the major cheilostome clades in Fig. 1, with the ancestral backbone node, and corresponding BS support, that gave rise to this clade highlighted with the matching color) of the inferred trimmed phylogeny**.** This is based on 721 taxa (690 cheilostomes) with 9170 nucleotide and amino acid characters (18 genes), and with bootstrap values (shown at nodes) inferred using RAxML. Tips are labelled with Taxon tags corresponding to Tables S1 and S2. *This figure is supplied as a separate file.*

**Fig. S2B. Phylogeny based on the trimmed alignment.** S2B shows the inferred maximum likelihood cladogram (the letters A through G correspond to the major cheilostome clades in Fig. 1, with the ancestral backbone node, and corresponding BS support, that gave rise to this clade highlighted with the matching color) of the inferred trimmed phylogeny**.** This is based on 721 taxa (690 cheilostomes) with 9170 nucleotide and amino acid characters (18 genes), and with bootstrap values (shown at nodes) inferred using RAxML. Tips are labelled with Taxon tags corresponding to Tables S1 and S2. *This figure is supplied as a separate file.*

**Fig. S3. Joint time priors for fossil calibration.** The topology is based on our trimmed tree (Fig. S2) and the plotted time priors based on "STL" are shown in grey and salmon-pink, where the latter are nodes used for calibration (roman numerals correspond to those in Table S4). The letters A through G correspond to the major cheilostome clades in Fig. 1. *This figure is supplied as a separate file.*

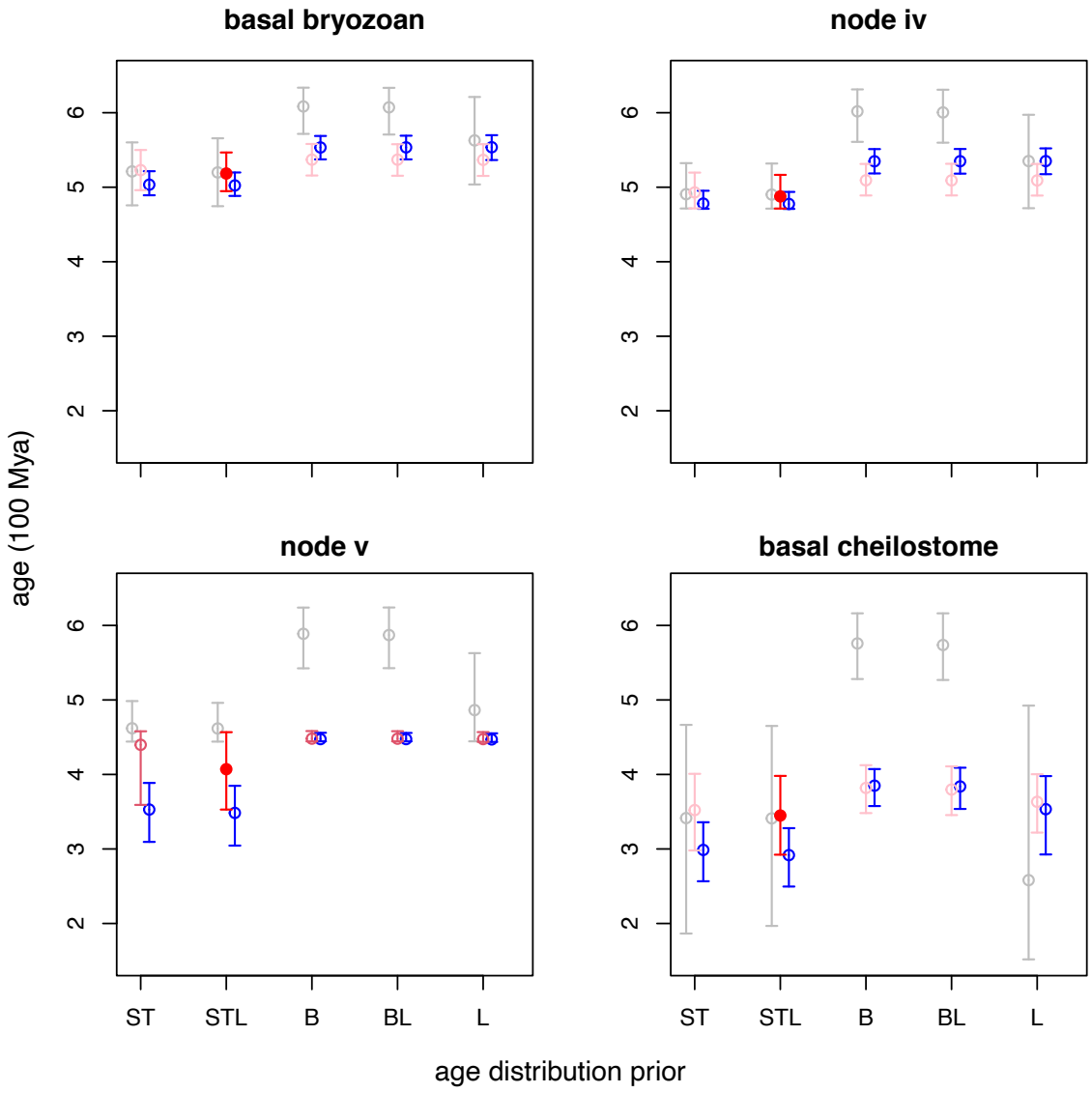


**Fig. S4. Different priors and clocks give similar age estimates.** Each panel show the five different fossil age calibrations used where grey points show the median for the joint prior, pink the posterior using an independent clock model (clock = 2 in MCMCTree) and blue using an autocorrelated clock model (clock = 3 in MCMCtree). The posteriors for the STL and clock 2 combination (highlighted in red among the pink) are those shown in Fig. 2. Lines show 95% credibility intervals. Node labels correspond to those in Fig. 2 and S3.

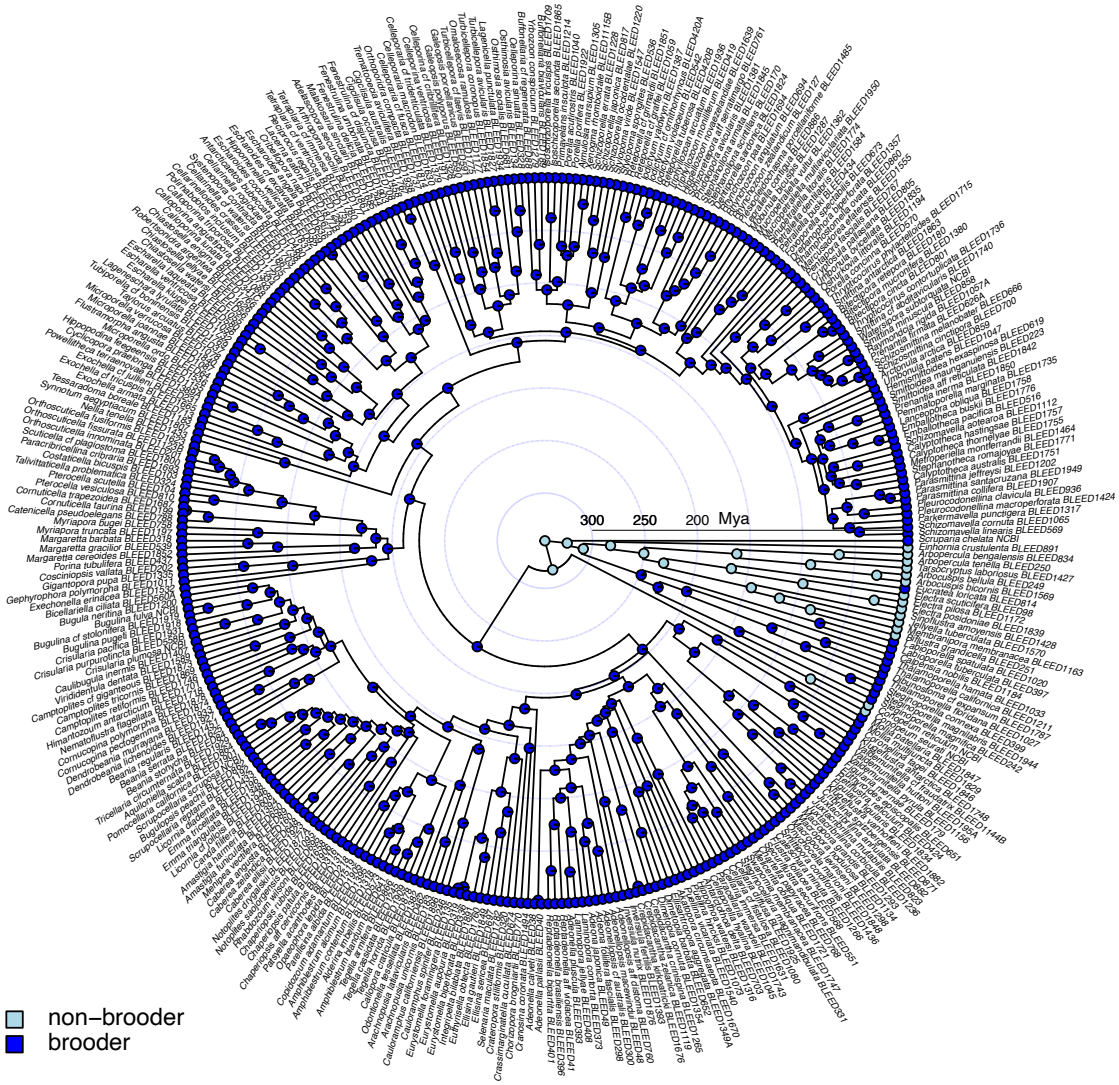


**Fig. S5. Reconstructed ancestral (non)brooding states.** Ancestral reconstruction using trimmed tree and tip taxa non(brooding) with branch lengths estimated in millions of years (from "STL" calibration).

## Supplementary Tables

**Table S1. Metadata for specimen-vouchered and non-specimen sequences.** This table, *supplied as a separate excel file*, tabulates taxon and specimen information and gives locations with names (where available), latitudes (lat) and longitudes (long) and depths (m). Specimens donated from a museum or institute via a coauthor are also marked, and alternative codes that could help trace the sample are given where available. Collector and collection dates are given to the best of our knowledge. Gene bank accessions and voucher numbers associated with the Natural History Museum Oslo are given.

**Table S2. Genes included for samples.** This table, *supplied as a separate excel file*, shows the total number of mitochondrial (MT) and mitochondrial + 18S and 28S nuclear genes (TOTAL) and the availability of each gene (0 = unavailable, 1 = available) for our phylogenetic inference (Fig. S1). There are 854 taxa as these include also non-bryozoan outgroups. Taxon names and sample number (Taxon tag) are given where the BLEED sequences originated from our lab.

**Table S3. Accession numbers for inclusion from NCBI.** This table, *supplied as a separate excel file*, gives the NCBI accession numbers for previously published sequences we included in our tree, as well as their taxon names and sample number (Taxon tag), where the BLEED sequences originated from our lab.

1385

| Node | **MCMCTREE input** | Justification (see SM text for more references and details) |
|---|---|---|
| i | B(5.14,6.36,0.001,0.001)' | Pancrustacea = *Drosophila, Squilla, Triops*. The calibrated node is placed at the split between Pancrustaea and Chelicerata (*Limulus*) as Pancrustacea cannot be younger than the oldest pancrustacean fossil known at 514 Mya. This and all other nodes are conservatively constrained to being younger than the base of the tree, set to be the bilaterian maximum at 636 MYA (see SM text) |
| | L(5.14, 0.1,0.5,0.001)' | |
| | ST(5.14,0.193,50,1)' | |
| ii | 'B(4.77,6.36,0.001,0.001)' | Annelida = *Urechis, Platyneris, Perionyx*. The calibrated node is placed at the split between Annelida and Sipunulida (*Sipunculus*) Annelida cannot be younger than the oldest annelid fossil known at 477 Mya (see SM text) |
| | 'L(4.77,0.1,0.5,0.001)' | |
| | 'ST(4.77,0.252,50,1)' | |
| iii | 'B(5.21,6.36,0.001,0.001)' | Brachiopoda = *Terebratulina*, *Terebratalia*, *Laqueus*. The calibrated node is placed at the split between Brachiopoda and Bryozoa as Brachiopoda cannot be younger than the oldest brachiopod fossil known at Cambrian Stage 2 (lower limit = 521 Mya). We use the upper bound of the stratigraphic stages, e.g. here it will be the upper bound of Cambrian 2 at 521 Mya. |
| | 'L(5.21,0.1,0.5,0.001)' | |
| | 'ST(5.21,0.182,50,1)' | |
| iv | 'B(4.72,6.36,0.001,0.001)' | The split between cyclostomes and extant ctenostomes and cheilostomes cannot be younger than the oldest cyclostome fossil *Wolinella baltica* Dzik, 1981 as we do not believe members of crown cyclostomes could have given rise to ctenostomes or cheilostomes. This logic is applicable also to other cheilsotome nodes. |
| | 'L(4.72,0.1,0.5,0.001)' | |
| | 'ST(4.72,0.26,50,1)' | |
| v | 'B(4.45,6.36,0.001,0.001)' | The split between ctenostomes and cheilostomes cannot be younger than the oldest ctenostome fossil *Ropalonaria venosa* Ulrich, 1879 |
| | 'L(4.45,0.1,0.5,0.001)' | |
| | 'ST(4.45,0.303,50,1)' | |
| vi | 'B(1.52,6.36,0.001,0.001)' | The base of cheilostomes cannot be younger the oldest cheilostome fossil *Pyriporopsis pohowskyi* Taylor, 1994 |
| | 'L(1.52,0.1,0.5,0.001)' | |
| | 'ST(1.52,0.767,50,1)' | |
| vii | 'B(0.41,6.36,0.001,0.001)' | The base of Thalamoporellina (*Labioporella, Steginoporella, Thalamoporella*) cannot be younger than oldest fossils of the group all found in the Lutetian. |
| | 'L(0.41,0.1,0.5,0.001)' | |
| | 'ST(0.41,0.942,50,1)' | |
| viii | 'B(0.72,6.36,0.001,0.001)' | The split of *Lunularia* from other genera cannot be younger than the oldest *Lunularia* fossil. |
| | 'L(0.72,0.1,0.5,0.001)' | |
| | 'ST(0.72,0.893,50,1)' | |
| ix | 'B(0.66,6.36,0.001,0.001)' | The split of *Electra* from *Eucratea* cannot be younger than the oldest *Electra* fossil |
| | 'L(0.66,0.1,0.5,0.001)' | |
| | 'ST(0.66,0.903,50,1)' | |
| x | B(0.66,6.36,0.001,0.001)' | 'The base of Monoporelloidea (*Macropora* and *Monoporella*) cannot be younger |

| | | |
|---|---|---|
| | L(0.66,0.1,0.5,0.001)' | than the oldest Monoporelloidea fossil *Monoporella* sp. from the Campanian–Maastrichtian. |
| | ST[0.66~0.903~50~1] | |
| xi | 'B(0.66,6.36,0.001,0.001)' | The split of *Celleria* (including *Paracellaria* which is morphologically a *Cellaria*) from *Swanomia* cannot be younger than the oldest *Cellaria* fossil. |
| | 'L(0.66,0.1,0.5,0.001)' | |
| | 'ST(0.66,0.903,50,1)' | |
| xii | 'B(0.52,6.36,0.001,0.001)' | The base of the adeonids (*Adeonellopsis* to *Reptadeonella*) cannot be younger than oldest fossil of the group, which is from the Ypresian. |
| | 'L(0.52,0.1,0.5,0.001)' | |
| | 'ST(0.52,0.925,50,1)' | |
| xiii | 'B(0.66,6.36,0.001,0.001)' | The split of *Nellia* from other genera cannot be younger than the oldest *Nellia* fossil. |
| | 'L(0.66,0.1,0.5,0.001)' | |
| | 'ST(0.66,0.903,50,1)' | |
| xiv | 'B(0.20,6.36,0.001,0.001)' | The split of *Microporella* (including *Flustramorpha*) from other genera cannot be younger than the oldest microporellid fossil. |
| | 'L(0.20,0.1,0.5,0.001)' | |
| | 'ST(0.20,0.976,50,1)' | |
| xv | 'B(0.16,6.36,0.001,0.001)' 'L(0.16,0.1,0.5,0.001)' 'ST(0.16,0.982,50,1)' | The split of *Fenestrulina* from other genera cannot be younger than the oldest *Fenestrulina* fossil. |
| xvi | 'B(0.52,6.36,0.001,0.001)' | The base of Celleporidae (*Celleporaria*…to…*Celleporina*) cannot be younger than the oldest Celleporidae fossil |
| | 'L(0.52,0.1,0.5,0.001)' | |
| | 'ST(0.52,0.925,50,1)' | |
| xvii | 'B(0.52,6.36,0.001,0.001)' | The split of Philodoporidae (*Plesiocleidochasma*…to...*Phidolopora*) cannot be younger than the oldest Philodoporidae fossil |
| | 'L(0.52,0.1,0.5,0.001)' | |
| | 'ST(0.52,0.925,50,1)' | |
| xviii | 'B(0.41,6.36,0.001,0.001)' | The split of *Parasmittina* (including the morphologically equivalent *Pleurocodonellina*) from other genera cannot be younger than the oldest *Parasmittina* fossil. |
| | 'L(0.41,0.1,0.5,0.001)' | |
| | 'ST(0.41,0.942,50,1)' | |

**Table S4. Fossil calibrations.** We state and justify the fossil calibration nodes used. Each of the nodes used in calibration have the same roman numerals in Fig. 2 and Fig. S3. The second column gives the input used in MCMCTree for the "ST", "L" and "B" prior age distributions. Note that for "STL" we simply used "ST" for all nodes, except node i, which is constraint to be "L". The same goes for "BL". Posteriors from the five differering shapes of priors are shown in Fig. S4 for four key nodes. This Table spans two pages.

**Table S5. Brooding states.** This table, *supplied as a separate excel file*, presents the state of parental care for the named taxon and sample (Taxon tag) where 0 = non-brooding and 1 = brooding, used in ancestral state reconstruction and HiSSE analyses. Note that we are here using the term "brooding" to mean both viviparity (e.g. *Synnotum*) and external brooding (e.g. *Microporella* with calcified ovicells or *Eucratea* with an external membranous brood sac) as all "brooders" have non-planktotrophic larvae. Likewise non-incubating (non-brooding in the terminology used in this contribution) cheilostome taxa have planktotrophic (feeding) larvae.

| M | P | Wt | T | Tau | Eps | Transition parameters (q) | | | | | | | |
|---|---|---|---|---|---|---|---|---|---|---|---|---|---|
| | | | | | | 01 | | 10 | | AB | | BA | |
| Null | 4 | 5.20E- | NA | 5.87 (4.19, 8.92) | 0.37 | 0.04 (0.03, 0.08) | | 0 (0, 0) | | NA | | NA | |
| BiSSE | 5 | 4.22E-04 | 0 | 3.21 (2.45, 4.73) | 0.21 (0.12, | 0.04(0.03,0.09) | | 0 (0,0) | | NA | | NA | |
| | | | 1 | 4.55 (3.46, 6.02) | | | | | | | | | |
| | | | | | | 0A1A | 0B1B | 1A0A | 1B0B | 0A0B | 1A1B | 0B0A | 1B1A |
| Cid2* | 6 | 0.58 | 0A | 5.53(3.91, 6.45) | 0.24 (0.11, 0.30) | 0.04 (0.02, 0.07) | | 0 (0,0) | | 0.02(0.10, 0.38) | | | |
| | | | 1A | | | | | | | | | | |
| | | | 0B | 3.24(2.05, 3.85) | | | | | | | | | |
| | | | 1B | | | | | | | | | | |
| | | | | | | 0A1A group | | 1A0A group | | 0A0B and q1A1B group | | | |
| Cid4 | 8 | 0.04 | 0A | 3.55 (1.15, 5.37) | 0(0,0) | 0.04(0.01, 0.08) | | 0 (0, 0.1) | | 0.09(0.05, 0.27) | | | |
| | | | 1A | | | | | | | | | | |
| | | | 0B | 3.66 (1.00, 5.11) | | | | | | | | | |
| | | | 1B | | | | | | | | | | |
| | | | 0C | 1.49 (1.18, 5.14) | | | | | | | | | |
| | | | 1C | | | | | | | | | | |
| | | | 0D | 2.04 (1.39, 4.27) | | | | | | | | | |
| | | | 1D | | | | | | | | | | |
| | | | | | | 0A1A | 0B1B | 1A0A | 1B0B | 0A0B | 1A1B | 0B0A | 1B1A |
| HiSSE | 10 | 0.02 | 0A | 2.97 (2.03, 3.73) | 0.11(0.04, 0.15) | 0.05(0.03, 0.8) | 0(0,0) | 0 (0,0) | 0 (0,0) | 0.30 (0.12, 0.57) | | 0.30(0.12, 0.57) | |
| | | | 1A | 2.67 (1.91, 3.37) | | | | | | | | | |
| | | | 0B | 0 (0, 0) | | | | | | | | | |
| | | | 1B | 4.44 (3.58, 5.26) | | | | | | | | | |

**Table S6. SSE Parameters.** This table presents parameter estimates from BiSSE, HiSSE and their null models (listed in the first column). The log likelihood (Loglik), number of different parameters (no. Params.) and the AIC model weights are given for each model (also shown in Table 1), followed by the traits that are assigned separate extinction and speciation rates. Here, 0 and 1 represent non-brooding and brooding respectively, while letters (A to D) represent hidden states combined with brooding or non-brooding. Tau represents birth+death or "turnover" while eps = death/birth or "extinction fraction", which are estimated in HiSSE (*41*). The transition parameters (q) are written as transitioning from the first to the second, i.e. q01 means the transition from state 0 (non-brooding) to 1 (brooding). Numbers are means, while those in parentheses are 95% CI given to 2 decimal places). Cid2 is the best model by AIC criterion and marked with an *, although Cid4 is not far behind.

| | Model weights | | |
|---|---|---|---|
| Model: Topology | Main text topology | *Lunularia* removed | "Basal" *Conopeum* |
| Null | 5.20E-06 | 3.38E.07 | 2.63E-09 |
| BiSSE | 4.22E-04 | 1.56E-05 | 0.010 |
| cid2 (BiSSE null) | **0.581** | 0.084 | 1.17E-07 |
| cid4 (HiSSE null) | 0.402 | 0.075 | 1.58E-06 |
| HiSSE | 0.017 | **0.841** | **0.980** |
| | Instances estimated | | |
| non-brooding --> brooding | 5.10 | 4.20 | 5.12 |

**Table S7. Model weights for alternative topologies.** This table shows AIC model weights of the five diversification trait models (equivalent to Table 1 in main text) for two alternative topologies, one where *Lunularia* has been removed and one where *Conopeum* is alternatively placed as sister to all other extant cheilostomes ("Basal" *Conopeum*).